Experimental quantum teleportation

Dik Bouwmeester, Jian-Wei Pan, Klaus Mattle, Manfred Eibl, Harald Weinfurter & Anton Zeilinger

Institut für Experimentalphysik, Universität Innsbruck, Technikerstr. 25, A-6020 Innsbruck, Austria

Quantum teleportation—the transmission and reconstruction over arbitrary distances of the state of a quantum system—is demonstrated experimentally. During teleportation, an initial photon which carries the polarization that is to be transferred and one of a pair of entangled photons are subjected to a measurement such that the second photon of the entangled pair acquires the polarization of the initial photon. This latter photon can be arbitrarily far away from the initial one. Quantum teleportation will be a critical ingredient for quantum computation networks.

The dream of teleportation is to be able to travel by simply reappearing at some distant location. An object to be teleported can be fully characterized by its properties, which in classical physics can be determined by measurement. To make a copy of that object at a distant location one does not need the original parts and pieces—all that is needed is to send the scanned information so that it can be used for reconstructing the object. But how precisely can this be a true copy of the original? What if these parts and pieces are electrons, atoms and molecules? What happens to their individual quantum properties, which according to the Heisenberg's uncertainty principle cannot be measured with arbitrary precision?

Bennett *et al.*[1] have suggested that it is possible to transfer the quantum state of a particle onto another particle—the process of quantum teleportation—provided one does not get any information about the state in the course of this transformation. This requirement can be fulfilled by using entanglement, the essential feature of quantum mechanics[2]. It describes correlations between quantum systems much stronger than any classical correlation could be.

The possibility of transferring quantum information is one of the cornerstones of the emerging field of quantum communication and quantum computation[3]. Although there is fast progress in the theoretical description of quantum information processing, the difficulties in handling quantum systems have not allowed an equal advance in the experimental realization of the new proposals. Besides the promising developments of quantum cryptography[4] (the first provably secure way to send secret messages), we have only recently succeeded in demonstrating the possibility of quantum dense coding[5], a way to quantum mechanically enhance data compression. The main reason for this slow experimental progress is that, although there exist methods to produce pairs of entangled photons[6], entanglement has been demonstrated for atoms only very recently[7] and it has not been possible thus far to produce entangled states of more than two quanta.

Here we report the first experimental verification of quantum teleportation. By producing pairs of entangled photons by the process of parametric down-conversion and using two-photon interferometry for analysing entanglement, we could transfer a quantum property (in our case the polarization state) from one photon to another. The methods developed for this experiment will be of great importance both for exploring the field of quantum communication and for future experiments on the foundations of quantum mechanics.

The problem

To make the problem of transferring quantum information clearer, suppose that Alice has some particle in a certain quantum state $|\psi\rangle$ and she wants Bob, at a distant location, to have a particle in that state. There is certainly the possibility of sending Bob the particle directly. But suppose that the communication channel between Alice and Bob is not good enough to preserve the necessary quantum coherence or suppose that this would take too much time, which could easily be the case if $|\psi\rangle$ is the state of a more complicated or massive object. Then, what strategy can Alice and Bob pursue?

As mentioned above, no measurement that Alice can perform on $|\psi\rangle$ will be sufficient for Bob to reconstruct the state because the state of a quantum system cannot be fully determined by measurements. Quantum systems are so evasive because they can be in a superposition of several states at the same time. A measurement on the quantum system will force it into only one of these states—this is often referred to as the projection postulate. We can illustrate this important quantum feature by taking a single photon, which can be horizontally or vertically polarized, indicated by the states $|\leftrightarrow\rangle$ and $|\updownarrow\rangle$. It can even be polarized in the general superposition of these two states

$$|\psi\rangle = \alpha|\leftrightarrow\rangle + \beta|\updownarrow\rangle \qquad (1)$$

where α and β are two complex numbers satisfying $|\alpha|^2 + |\beta|^2 = 1$. To place this example in a more general setting we can replace the states $|\leftrightarrow\rangle$ and $|\updownarrow\rangle$ in equation (1) by $|0\rangle$ and $|1\rangle$, which refer to the states of any two-state quantum system. Superpositions of $|0\rangle$ and $|1\rangle$ are called qubits to signify the new possibilities introduced by quantum physics into information science[8].

If a photon in state $|\psi\rangle$ passes through a polarizing beamsplitter—a device that reflects (transmits) horizontally (vertically) polarized photons—it will be found in the reflected (transmitted) beam with probability $|\alpha|^2$ ($|\beta|^2$). Then the general state $|\psi\rangle$ has been projected either onto $|\leftrightarrow\rangle$ or onto $|\updownarrow\rangle$ by the action of the measurement. We conclude that the rules of quantum mechanics, in particular the projection postulate, make it impossible for Alice to perform a measurement on $|\psi\rangle$ by which she would obtain all the information necessary to reconstruct the state.

The concept of quantum teleportation

Although the projection postulate in quantum mechanics seems to bring Alice's attempts to provide Bob with the state $|\psi\rangle$ to a halt, it was realised by Bennett *et al.*[1] that precisely this projection postulate enables teleportation of $|\psi\rangle$ from Alice to Bob. During teleportation Alice will destroy the quantum state at hand while Bob receives the quantum state, with neither Alice nor Bob obtaining information about the state $|\psi\rangle$. A key role in the teleportation scheme is played by an entangled ancillary pair of particles which will be initially shared by Alice and Bob.

Suppose particle 1 which Alice wants to teleport is in the initial state $|\psi\rangle_1 = \alpha|\leftrightarrow\rangle_1 + \beta|\updownarrow\rangle_1$ (Fig. 1a), and the entangled pair of particles 2 and 3 shared by Alice and Bob is in the state:

$$|\psi^-\rangle_{23} = \frac{1}{\sqrt{2}}\left(|\leftrightarrow\rangle_2|\updownarrow\rangle_3 - |\updownarrow\rangle_2|\leftrightarrow\rangle_3\right) \quad (2)$$

That entangled pair is a single quantum system in an equal superposition of the states $|\leftrightarrow\rangle_2|\updownarrow\rangle_3$ and $|\updownarrow\rangle_2|\leftrightarrow\rangle_3$. The entangled state contains no information on the individual particles; it only indicates that the two particles will be in opposite states. The important property of an entangled pair is that as soon as a measurement on one of the particles projects it, say, onto $|\leftrightarrow\rangle$ the state of the other one is determined to be $|\updownarrow\rangle$, and vice versa. How could a measurement on one of the particles instantaneously influence the state of the other particle, which can be arbitrarily far away? Einstein, among many other distinguished physicists, could simply not accept this "spooky action at a distance". But this property of entangled states has now been demonstrated by numerous experiments (for reviews, see refs 9, 10).

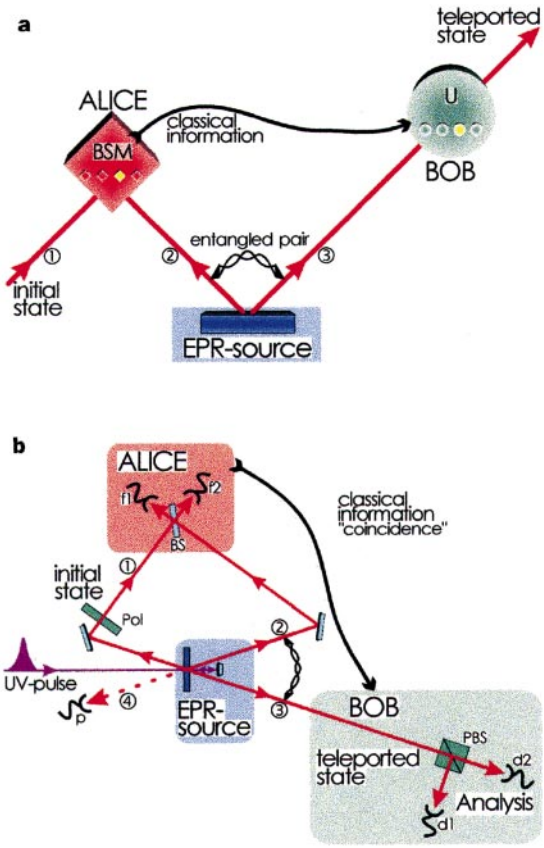

Figure 1 Scheme showing principles involved in quantum teleportation (**a**) and the experimental set-up (**b**). **a**, Alice has a quantum system, particle 1, in an initial state which she wants to teleport to Bob. Alice and Bob also share an ancillary entangled pair of particles 2 and 3 emitted by an Einstein–Podolsky–Rosen (EPR) source. Alice then performs a joint Bell-state measurement (BSM) on the initial particle and one of the ancillaries, projecting them also onto an entangled state. After she has sent the result of her measurement as classical information to Bob, he can perform a unitary transformation (U) on the other ancillary particle resulting in it being in the state of the original particle. **b**, A pulse of ultraviolet radiation passing through a nonlinear crystal creates the ancillary pair of photons 2 and 3. After retroflection during its second passage through the crystal the ultraviolet pulse creates another pair of photons, one of which will be prepared in the initial state of photon 1 to be teleported, the other one serving as a trigger indicating that a photon to be teleported is under way. Alice then looks for coincidences after a beam splitter BS where the initial photon and one of the ancillaries are superposed. Bob, after receiving the classical information that Alice obtained a coincidence count in detectors f1 and f2 identifying the $|\psi^-\rangle_{12}$ Bell state, knows that his photon 3 is in the initial state of photon 1 which he then can check using polarization analysis with the polarizing beam splitter PBS and the detectors d1 and d2. The detector p provides the information that photon 1 is under way.

The teleportation scheme works as follows. Alice has the particle 1 in the initial state $|\psi\rangle_1$ and particle 2. Particle 2 is entangled with particle 3 in the hands of Bob. The essential point is to perform a specific measurement on particles 1 and 2 which projects them onto the entangled state:

$$|\psi^-\rangle_{12} = \frac{1}{\sqrt{2}}\left(|\leftrightarrow\rangle_1|\updownarrow\rangle_2 - |\updownarrow\rangle_1|\leftrightarrow\rangle_2\right) \quad (3)$$

This is only one of four possible maximally entangled states into which any state of two particles can be decomposed. The projection of an arbitrary state of two particles onto the basis of the four states is called a Bell-state measurement. The state given in equation (3) distinguishes itself from the three other maximally entangled states by the fact that it changes sign upon interchanging particle 1 and particle 2. This unique antisymmetric feature of $|\psi^-\rangle_{12}$ will play an important role in the experimental identification, that is, in measurements of this state.

Quantum physics predicts[1] that once particles 1 and 2 are projected into $|\psi^-\rangle_{12}$, particle 3 is instantaneously projected into the initial state of particle 1. The reason for this is as follows. Because we observe particles 1 and 2 in the state $|\psi^-\rangle_{12}$ we know that whatever the state of particle 1 is, particle 2 must be in the opposite state, that is, in the state orthogonal to the state of particle 1. But we had initially prepared particle 2 and 3 in the state $|\psi^-\rangle_{23}$, which means that particle 2 is also orthogonal to particle 3. This is only possible if particle 3 is in the same state as particle 1 was initially. The final state of particle 3 is therefore:

$$|\psi\rangle_3 = \alpha|\leftrightarrow\rangle_3 + \beta|\updownarrow\rangle_3 \quad (4)$$

We note that during the Bell-state measurement particle 1 loses its identity because it becomes entangled with particle 2. Therefore the state $|\psi\rangle_1$ is destroyed on Alice's side during teleportation.

This result (equation (4)) deserves some further comments. The transfer of quantum information from particle 1 to particle 3 can happen over arbitrary distances, hence the name teleportation. Experimentally, quantum entanglement has been shown[11] to survive over distances of the order of 10 km. We note that in the teleportation scheme it is not necessary for Alice to know where Bob is. Furthermore, the initial state of particle 1 can be completely unknown not only to Alice but to anyone. It could even be quantum mechanically completely undefined at the time the Bell-state measurement takes place. This is the case when, as already remarked by Bennett *et al.*[1], particle 1 itself is a member of an entangled pair and therefore has no well-defined properties on its own. This ultimately leads to entanglement swapping[12,13].

It is also important to notice that the Bell-state measurement does not reveal any information on the properties of any of the particles. This is the very reason why quantum teleportation using coherent two-particle superpositions works, while any measurement on one-particle superpositions would fail. The fact that no information whatsoever is gained on either particle is also the reason why quantum teleportation escapes the verdict of the no-cloning theorem[14]. After successful teleportation particle 1 is not available in its original state any more, and therefore particle 3 is not a clone but is really the result of teleportation.

A complete Bell-state measurement can not only give the result that the two particles 1 and 2 are in the antisymmetric state, but with equal probabilities of 25% we could find them in any one of the three other entangled states. When this happens, particle 3 is left in one of three different states. It can then be brought by Bob into the original state of particle 1 by an accordingly chosen transformation, independent of the state of particle 1, after receiving via a classical communication channel the information on which of the Bell-state

results was obtained by Alice. Yet we note, with emphasis, that even if we chose to identify only one of the four Bell states as discussed above, teleportation is successfully achieved, albeit only in a quarter of the cases.

Experimental realization

Teleportation necessitates both production and measurement of entangled states; these are the two most challenging tasks for any experimental realization. Thus far there are only a few experimental techniques by which one can prepare entangled states, and there exist no experimentally realized procedures to identify all four Bell states for any kind of quantum system. However, entangled pairs of photons can readily be generated and they can be projected onto at least two of the four Bell states.

We produced the entangled photons 2 and 3 by parametric down-conversion. In this technique, inside a nonlinear crystal, an incoming pump photon can decay spontaneously into two photons which, in the case of type II parametric down-conversion, are in the state given by equation (2) (Fig. 2)[6].

To achieve projection of photons 1 and 2 into a Bell state we have to make them indistinguishable. To achieve this indistinguishability we superpose the two photons at a beam splitter (Fig. 1b). Then if they are incident one from each side, how can it happen that they emerge still one on each side? Clearly this can happen if they are either both reflected or both transmitted. In quantum physics we have to superimpose the amplitudes for these two possibilities. Unitarity implies that the amplitude for both photons being reflected obtains an additional minus sign. Therefore, it seems that the two processes cancel each other. This is, however, only true for a symmetric input state. For an antisymmetric state, the two possibilities obtain another relative minus sign, and therefore they constructively interfere[15,16]. It is thus sufficient for projecting photons 1 and 2 onto the antisymmetric state $|\psi^-\rangle_{12}$ to place detectors in each of the outputs of the beam splitter and to register simultaneous detections (coincidence)[17–19].

To make sure that photons 1 and 2 cannot be distinguished by their arrival times, they were generated using a pulsed pump beam and sent through narrow-bandwidth filters producing a coherence time much longer than the pump pulse length[20]. In the experiment, the pump pulses had a duration of 200 fs at a repetition rate of 76 MHz. Observing the down-converted photons at a wavelength of 788 nm and a bandwidth of 4 nm results in a coherence time of 520 fs. It should be mentioned that, because photon 1 is also produced as part of an entangled pair, its partner can serve to indicate that it was emitted.

How can one experimentally prove that an unknown quantum state can be teleported? First, one has to show that teleportation works for a (complete) basis, a set of known states into which any other state can be decomposed. A basis for polarization states has just two components, and in principle we could choose as the basis horizontal and vertical polarization as emitted by the source. Yet this would not demonstrate that teleportation works for any general superposition, because these two directions are preferred directions in our experiment. Therefore, in the first demonstration we choose as the basis for teleportation the two states linearly polarized at −45° and +45° which are already superpositions of the horizontal and vertical polarizations. Second, one has to show that teleportation works for superpositions of these base states. Therefore we also demonstrate teleportation for circular polarization.

Results

In the first experiment photon 1 is polarized at 45°. Teleportation should work as soon as photon 1 and 2 are detected in the $|\psi^-\rangle_{12}$ state, which occurs in 25% of all possible cases. The $|\psi^-\rangle_{12}$ state is identified by recording a coincidence between two detectors, f1 and f2, placed behind the beam splitter (Fig. 1b).

If we detect a f1f2 coincidence (between detectors f1 and f2), then photon 3 should also be polarized at 45°. The polarization of photon 3 is analysed by passing it through a polarizing beam splitter selecting +45° and −45° polarization. To demonstrate teleportation, only detector d2 at the +45° output of the polarizing beam splitter should click (that is, register a detection) once detectors f1 and f2 click. Detector d1 at the −45° output of the polarizing beam splitter should not detect a photon. Therefore, recording a three-fold coincidence d2f1f2 (+45° analysis) together with the absence of a three-fold coincidence d1f1f2 (−45° analysis) is a proof that the polarization of photon 1 has been teleported to photon 3.

To meet the condition of temporal overlap, we change in small

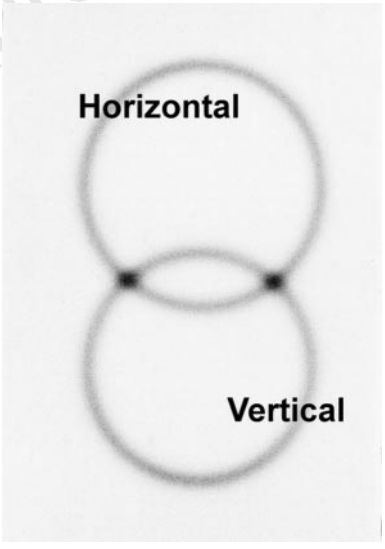

Figure 2 Photons emerging from type II down-conversion (see text). Photograph taken perpendicular to the propagation direction. Photons are produced in pairs. A photon on the top circle is horizontally polarized while its exactly opposite partner in the bottom circle is vertically polarized. At the intersection points their polarizations are undefined; all that is known is that they have to be different, which results in entanglement.

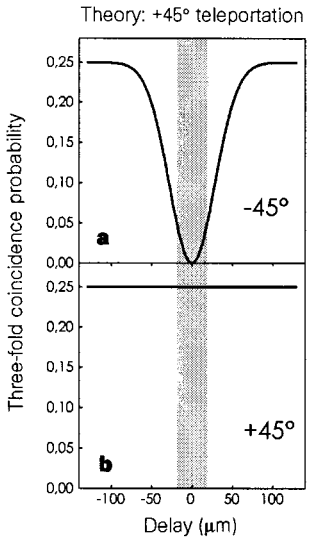

Figure 3 Theoretical prediction for the three-fold coincidence probability between the two Bell-state detectors (f1, f2) and one of the detectors analysing the teleported state. The signature of teleportation of a photon polarization state at +45° is a dip to zero at zero delay in the three-fold coincidence rate with the detector analysing –45° (d1f1f2) (**a**) and a constant value for the detector analysis +45° (d2f1f2) (**b**). The shaded area indicates the region of teleportation.

steps the arrival time of photon 2 by changing the delay between the first and second down-conversion by translating the retroflection mirror (Fig. 1b). In this way we scan into the region of temporal overlap at the beam splitter so that teleportation should occur.

Outside the region of teleportation, photon 1 and 2 each will go either to f1 or to f2 independent of one another. The probability of having a coincidence between f1 and f2 is therefore 50%, which is twice as high as inside the region of teleportation. Photon 3 should not have a well-defined polarization because it is part of an entangled pair. Therefore, d1 and d2 have both a 50% chance of receiving photon 3. This simple argument yields a 25% probability both for the −45° analysis (d1f1f2 coincidences) and for the +45° analysis (d2f1f2 coincidences) outside the region of teleportation. Figure 3 summarizes the predictions as a function of the delay. Successful teleportation of the +45° polarization state is then characterized by a decrease to zero in the −45° analysis (Fig. 3a), and by a constant value for the +45° analysis (Fig. 3b).

The theoretical prediction of Fig. 3 may easily be understood by realizing that at zero delay there is a decrease to half in the coincidence rate for the two detectors of the Bell-state analyser, f1 and f2, compared with outside the region of teleportation. Therefore, if the polarization of photon 3 were completely uncorrelated to the others the three-fold coincidence should also show this dip to half. That the right state is teleported is indicated by the fact that the dip goes to zero in Fig. 3a and that it is filled to a flat curve in Fig. 3b.

We note that equally as likely as the production of photons 1, 2 and 3 is the emission of two pairs of down-converted photons by a single source. Although there is no photon coming from the first source (photon 1 is absent), there will still be a significant contribution to the three-fold coincidence rates. These coincidences have nothing to do with teleportation and can be identified by blocking the path of photon 1.

The probability for this process to yield spurious two- and three-fold coincidences can be estimated by taking into account the experimental parameters. The experimentally determined value for the percentage of spurious three-fold coincidences is 68% ± 1%. In the experimental graphs of Fig. 4 we have subtracted the experimentally determined spurious coincidences.

Table 1 Visibility of teleportation in three fold coincidences

Polarization	Visibility
+45°	0.63 ± 0.02
−45°	0.64 ± 0.02
0°	0.66 ± 0.02
90°	0.61 ± 0.02
Circular	0.57 ± 0.02

The experimental results for teleportation of photons polarized under +45° are shown in the left-hand column of Fig. 4; Fig. 4a and b should be compared with the theoretical predictions shown in Fig. 3. The strong decrease in the −45° analysis, and the constant signal for the +45° analysis, indicate that photon 3 is polarized along the direction of photon 1, confirming teleportation.

The results for photon 1 polarized at −45° demonstrate that teleportation works for a complete basis for polarization states (right-hand column of Fig. 4). To rule out any classical explanation for the experimental results, we have produced further confirmation that our procedure works by additional experiments. In these experiments we teleported photons linearly polarized at 0° and at 90°, and also teleported circularly polarized photons. The experimental results are summarized in Table 1, where we list the visibility of the dip in three-fold coincidences, which occurs for analysis orthogonal to the input polarization.

As mentioned above, the values for the visibilities are obtained after subtracting the offset caused by spurious three-fold coincidences. These can experimentally be excluded by conditioning the three-fold coincidences on the detection of photon 4, which effectively projects photon 1 into a single-particle state. We have performed this four-fold coincidence measurement for the case of teleportation of the +45° and +90° polarization states, that is, for two non-orthogonal

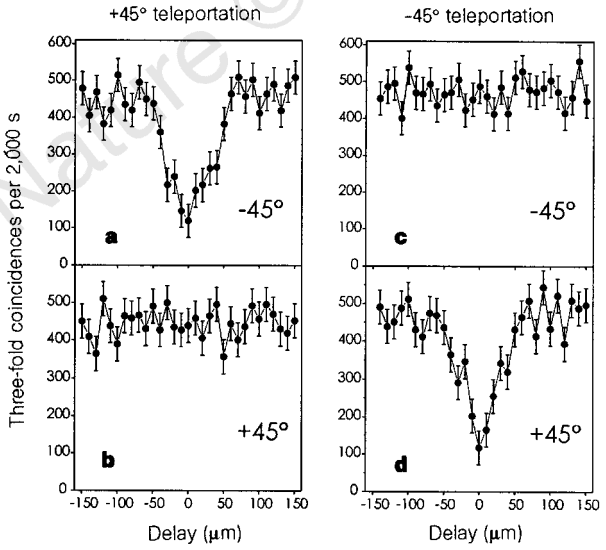

Figure 4 Experimental results. Measured three-fold coincidence rates d1f1f2 (−45°) and d2f1f2 (+45°) in the case that the photon state to be teleported is polarized at +45° (**a** and **b**) or at −45° (**c** and **d**). The coincidence rates are plotted as function of the delay between the arrival of photon 1 and 2 at Alice's beam splitter (see Fig. 1b). The three-fold coincidence rates are plotted after subtracting the spurious three-fold contribution (see text). These data, compared with Fig. 3, together with similar ones for other polarizations (Table 1) confirm teleportation for an arbitrary state.

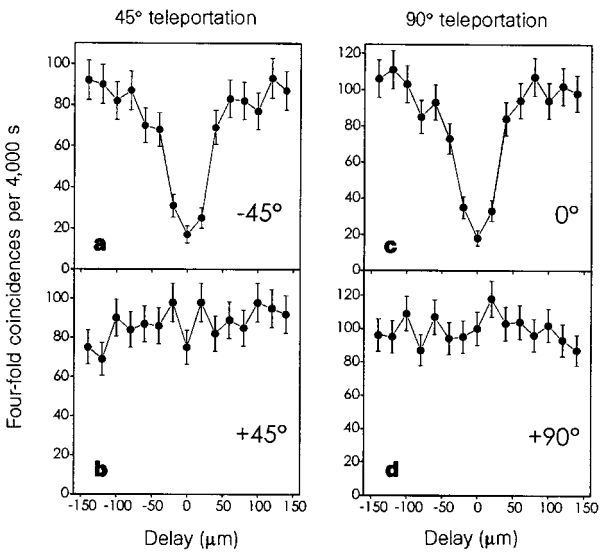

Figure 5 Four-fold coincidence rates (without background subtraction). Conditioning the three-fold coincidences as shown in Fig. 4 on the registration of photon 4 (see Fig. 1b) eliminates the spurious three-fold background. **a** and **b** show the four-fold coincidence measurements for the case of teleportation of the +45° polarization state; **c** and **d** show the results for the +90° polarization state. The visibilities, and thus the polarizations of the teleported photons, obtained without any background subtraction are 70% ± 3%. These results for teleportation of two non-orthogonal states prove that we have demonstrated teleportation of the quantum state of a single photon.

states. The experimental results are shown in Fig. 5. Visibilities of 70% ± 3% are obtained for the dips in the orthogonal polarization states. Here, these visibilities are directly the degree of polarization of the teleported photon in the right state. This proves that we have demonstrated teleportation of the quantum state of a single photon.

The next steps

In our experiment, we used pairs of polarization entangled photons as produced by pulsed down-conversion and two-photon interferometric methods to transfer the polarization state of one photon onto another one. But teleportation is by no means restricted to this system. In addition to pairs of entangled photons or entangled atoms[7,21], one could imagine entangling photons with atoms, or phonons with ions, and so on. Then teleportation would allow us to transfer the state of, for example, fast-decohering, short-lived particles, onto some more stable systems. This opens the possibility of quantum memories, where the information of incoming photons is stored on trapped ions, carefully shielded from the environment.

Furthermore, by using entanglement purification[22]—a scheme of improving the quality of entanglement if it was degraded by decoherence during storage or transmission of the particles over noisy channels—it becomes possible to teleport the quantum state of a particle to some place, even if the available quantum channels are of very poor quality and thus sending the particle itself would very probably destroy the fragile quantum state. The feasibility of preserving quantum states in a hostile environment will have great advantages in the realm of quantum computation. The teleportation scheme could also be used to provide links between quantum computers.

Quantum teleportation is not only an important ingredient in quantum information tasks; it also allows new types of experiments and investigations of the foundations of quantum mechanics. As any arbitrary state can be teleported, so can the fully undetermined state of a particle which is member of an entangled pair. Doing so, one transfers the entanglement between particles. This allows us not only to chain the transmission of quantum states over distances, where decoherence would have already destroyed the state completely, but it also enables us to perform a test of Bell's theorem on particles which do not share any common past, a new step in the investigation of the features of quantum mechanics. Last but not least, the discussion about the local realistic character of nature could be settled firmly if one used features of the experiment presented here to generate entanglement between more than two spatially separated particles[23,24]. □

Received 16 October; accepted 18 November 1997.

1. Bennett, C. H. *et al*. Teleporting an unknown quantum state via dual classic and Einstein-Podolsky-Rosen channels. *Phys. Rev. Lett.* **70,** 1895–1899 (1993).
2. Schrödinger, E. Die gegenwärtige Situation in der Quantenmechanik. *Naturwissenschaften* **23,** 807–812; 823–828; 844–849 (1935).
3. Bennett, C. H. Quantum information and computation. *Phys. Today* **48(10),** 24–30, October (1995).
4. Bennett, C. H., Brassard, G. & Ekert, A. K. Quantum Cryptography. *Sci. Am.* **267(4),** 50–57, October (1992).
5. Mattle, K., Weinfurter, H., Kwiat, P. G. & Zeilinger, A. Dense coding in experimental quantum communication. *Phys. Rev. Lett.* **76,** 4656–4659 (1996).
6. Kwiat, P. G. *et al*. New high intensity source of polarization-entangled photon pairs. *Phys. Rev. Lett.* **75,** 4337–4341 (1995).
7. Hagley, E. *et al*. Generation of Einstein-Podolsky-Rosen pairs of atoms. *Phys. Rev. Lett.* **79,** 1–5 (1997).
8. Schumacher, B. Quantum coding. *Phys. Rev. A* **51,** 2738–2747 (1995).
9. Clauser, J. F. & Shimony, A. Bell's theorem: experimental tests and implications. *Rep. Prog. Phys.* **41,** 1881–1927 (1978).
10. Greenberger, D. M., Horne, M. A. & Zeilinger, A. Multiparticle interferometry and the superposition principle. *Phys. Today* August, 22–29 (1993).
11. Tittel, W. *et al*. Experimental demonstration of quantum-correlations over more than 10 kilometers. *Phys. Rev. Lett.* (submitted).
12. Zukowski, M., Zeilinger, A., Horne, M. A. & Ekert, A. "Event-ready-detectors" Bell experiment via entanglement swapping. *Phys. Rev. Lett.* **71,** 4287–4290 (1993).
13. Bose, S., Vedral, V. & Knight, P. L. A multiparticle generalization of entanglement swapping. preprint.
14. Wootters, W. K. & Zurek, W. H. A single quantum cannot be cloned. *Nature* **299,** 802–803 (1982).
15. Loudon, R. *Coherence and Quantum Optics VI* (eds Everly, J. H. & Mandel, L.) 703–708 (Plenum, New York, 1990).
16. Zeilinger, A., Bernstein, H. J. & Horne, M. A. Information transfer with two-state two-particle quantum systems. *J. Mod. Optics* **41,** 2375–2384 (1994).
17. Weinfurter, H. Experimental Bell-state analysis. *Europhys. Lett.* **25,** 559–564 (1994).
18. Braunstein, S. L. & Mann, A. Measurement of the Bell operator and quantum teleportation. *Phys. Rev. A* **51,** R1727–R1730 (1995).
19. Michler, M., Mattle, K., Weinfurter, H. & Zeilinger, A. Interferometric Bell-state analysis. *Phys. Rev. A* **53,** R1209–R1212 (1996).
20. Zukowski, M., Zeilinger, A. & Weinfurter, H. Entangling photons radiated by independent pulsed sources. *Ann. NY Acad. Sci.* **755,** 91–102 (1995).
21. Fry, E. S., Walther, T. & Li, S. Proposal for a loophole-free test of the Bell inequalities. *Phys. Rev. A* **52,** 4381–4395 (1995).
22. Bennett, C. H. *et al*.Purification of noisy entanglement and faithful teleportation via noisy channels. *Phys. Rev. Lett.* **76,** 722–725 (1996).
23. Greenberger, D. M., Horne, M. A., Shimony, A. & Zeilinger, A. Bell's theorem without inequalities. *Am. J. Phys.* **58,** 1131–1143 (1990).
24. Zeilinger, A., Horne, M. A., Weinfurter, H. & Zukowski, M. Three particle entanglements from two entangled pairs. *Phys. Rev. Lett.* **78,** 3031–3034 (1997).

Acknowledgements. We thank C. Bennett, I. Cirac, J. Rarity, W. Wootters and P. Zoller for discussions, and M. Zukowski for suggestions about various aspects of the experiments. This work was supported by the Austrian Science Foundation FWF, the Austrian Academy of Sciences, the TMR program of the European Union and the US NSF.

Correspondence and requests for materials should be addressed to D.B. (e-mail: Dik.Bouwmeester@uibk.ac.at).

PHYSICAL REVIEW
LETTERS

VOLUME 80 9 FEBRUARY 1998 NUMBER 6

Experimental Realization of Teleporting an Unknown Pure Quantum State via Dual Classical and Einstein-Podolsky-Rosen Channels

D. Boschi,[1] S. Branca,[1] F. De Martini,[1] L. Hardy,[1,2] and S. Popescu[3,4]
[1]*Dipartimento di Fisica, Istituto Nazionale di Fisica Nucleare, Istituto Nazionale di Fisica della Materia, Università "La Sapienza," Roma 00185, Italy*
[2]*Clarendon Laboratory, University of Oxford, Oxford OX1 3PU, United Kingdom*
[3]*Isaac Newton Institute, University of Cambridge, Cambridge CB3 0EH, United Kingdom*
[4]*BRIMS, Hewlett-Packard Laboratories, Bristol BS12 SQZ, United Kingdom*
(Received 28 July 1997)

We report on a quantum optical experimental implementation of teleportation of unknown pure quantum states. This realizes all of the nonlocal aspects of the original scheme proposed by Bennett *et al.* and is equivalent to it up to a local operation. We exhibit results for the teleportation of a linearly polarized state and of an elliptically polarized state. We show that the experimental results cannot be explained in terms of a classical channel alone. The Bell measurement in our experiment can distinguish between all four Bell states *simultaneously* allowing, in the ideal case, a 100% success rate of teleportation. [S0031-9007(97)05275-7]

PACS numbers: 03.65.Bz, 03.67.–a, 42.50.–p, 89.70.+c

In Ref. [1], Bennett *et al.* showed that an unknown quantum state can be "disassembled into, then later reconstructed from, purely classical information and purely nonclassical Einstein-Podolsky-Rosen (EPR) correlations." They called this process *teleportation.* In their scheme, a sender, traditionally called Alice, is given a state unknown to her. She also has one of two particles prepared in an EPR state (such as a singlet state). She performs a Bell measurement on the combined system of the unknown state and her EPR particle, and transmits the result of this measurement by a classical channel to Bob, who has the second of the EPR particles. Depending on the result of the measurement, Bob performs one of four possible unitary transformations on his particle and it will now be in the unknown state.

In the experiment reported in this paper we take an approach first suggested in [2] in which a total of two photons, rather than three, are used. The EPR state is realized by **k**-vector (or path) entanglement, and the polarization degree of freedom of one of the photons is employed for preparing the unknown state [3]. This avoids the difficulties associated with having three photons and, as will be seen below, makes the Bell measurement much more straightforward. However, this approach does place a restriction on us in that the preparer must prepare his state on one of the EPR photons, and so the unknown state cannot come from outside (i.e., this means that Alice is presented with an unknown pure state rather than with part of an entangled state). Nevertheless, the scheme described here realizes all the nonlocal aspects of the original teleportation scheme, and is equivalent to the original scheme up to a local operation (since, in principle, any unknown state of a particle from outside could be swapped onto the polarization degree of freedom of Alice's EPR particle by a local unitary operation [4]). In particular, as in the original scheme, we emphasize that if the preparer does not tell Alice what state he has prepared then there is no way Alice can find out what the state is.

It is worthwhile mentioning that this leads to a 100% success rate for the Bell measurement in the ideal case rather than 50% as in previously suggested schemes [5].

No experiment is perfect, so we need to known how good the experiment has to be before we can say we have quantum teleportation. Our objective is to show that the experimental results cannot be explained by a classical channel alone (that is, without an EPR pair). Thus,

consider the following scenario. With a probability of $\frac{1}{3}$ the preparer prepares one of the states $|\phi_a\rangle$ $(a = 1, 2, 3)$ which corresponds to equally spaced linearly polarized states at 0°, 120°, and −120°. He then gives this state to Alice (without telling her which one it is). Alice makes a measurement on it in an attempt to gain some information about the state. The most general measurement she can make is a positive operator valued measure [6]. She will never obtain more information if some of the positive operators are not of rank one, and thus we can take them all to be of rank one, that is proportional to projection operators. Let Alice's measurement have L outcomes labeled $l = 1, 2, \ldots, L$ and let the positive operator associated with outcome l be $|\varepsilon_l\rangle\langle\varepsilon_l|$. We require that

$$\sum_{l=1}^{L} |\varepsilon_l\rangle\langle\varepsilon_l| = I\,. \tag{1}$$

Note that, in general, the states $|\varepsilon_l\rangle$ are neither orthogonal to each other or normalized but rather form an overcomplete basis set. The probability of getting outcome l given that the state prepared is $|\phi_a\rangle$ is $|\langle\phi_a|\varepsilon_l\rangle|^2$. Alice sends the information l to Bob over the classical channel and Bob prepares a state $|\phi_l^c\rangle$ (the c denotes that the state has been "classically teleported"). This state is chosen so as to give the best chance of passing a test for the original state. Bob now passes this state onto a verifier. We suppose that the preparer has told the verifier which state he prepared and the verifier sets his apparatus to measure the projection operator, $|\phi_a\rangle\langle\phi_a|$, onto this state. The probability that the classically teleported state will pass the test in this case is $|\langle\phi_a|\phi_l^c\rangle|^2$. The average probability S of passing the test

$$S = \sum_{a,l} \tfrac{1}{3}|\langle\phi_a|\phi_l^c\rangle|^2\,|\langle\phi_a|\varepsilon_l\rangle|^2. \tag{2}$$

In the Appendix we show that this classical teleportation protocol must satisfy

$$S \le \tfrac{3}{4}\,. \tag{3}$$

To show that we have quantum teleportation we must show that the experimental results violate this inequality [7].

The experiment is shown in Fig. 1. Pairs of polarization entangled photons are created directly using type-II degenerate parametric down-conversion by the method described in Refs. [8,9]. The β-barium borate (BBO) crystal is pumped by a 200 mW UV cw argon laser with wavelength 351.1 nm. The down-converted photons have a wavelength of 702.2 nm. The state of the photons at this stage is $\frac{1}{\sqrt{2}}(|v\rangle_1|h\rangle_2 + |h\rangle_1|v\rangle_2)$. However, we want a **k**-vector entangled state so next we let each photon pass through a calcite crystal (C), after which the state becomes

$$\frac{1}{\sqrt{2}}\left(|a_1\rangle\,|a_2\rangle + |b_1\rangle\,|b_2\rangle\right)|v\rangle_1|h\rangle_2\,. \tag{4}$$

By this method a polarization entangled state has been converted into a **k**-vector entangled state. Here, $|a_1\rangle\,|v\rangle_1$, for example, represents the state of photon 1 in path a_1 and having vertical polarization. Since each photon has the same polarization in each of the two paths it can take, the polarization part of the state factors out of the **k**-vector entanglement. The EPR pair for the teleportation procedure is provided by this **k**-vector entanglement. By means of (zero order) quarter-wave plates oriented at some angle γ to the horizontal and Fresnel rhomb polarization rotators (R) acting in the same way on paths a_1 and b_1 as shown in Fig. 1, the polarization degree of freedom of photon 1 is used by the preparer to prepare the general state: $|\phi\rangle = \alpha|v\rangle_1 + \beta|h\rangle_1$. This is the state to be teleported. The state of the whole system is now

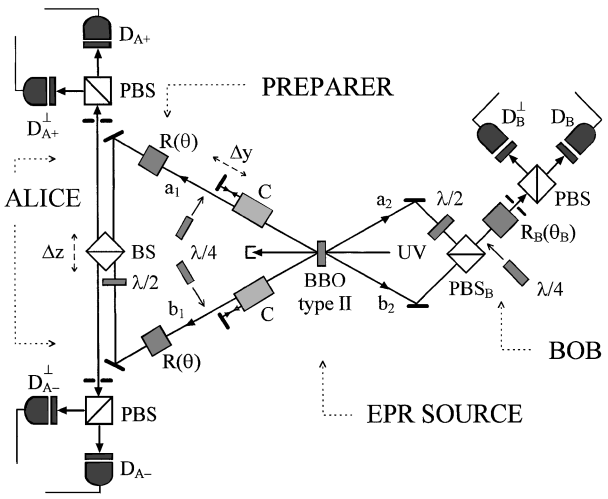

FIG. 1. Diagram of experimental setup showing the separate roles of the preparer, Alice, and Bob.

$$\frac{1}{\sqrt{2}}\left(|a_1\rangle\,|a_2\rangle + |b_1\rangle\,|b_2\rangle\right)\left(\alpha|v\rangle_1 + \beta|h\rangle_1\right)|h\rangle_2\,. \tag{5}$$

We now introduce four orthonormal states which are directly analogous to the Bell states considered in [1]:

$$|c_\pm\rangle = \frac{1}{\sqrt{2}}\left(|a_1\rangle\,|v\rangle_1 \pm |b_1\rangle\,|h\rangle_1\right), \tag{6}$$

$$|d_\pm\rangle = \frac{1}{\sqrt{2}}\left(|a_1\rangle\,|h\rangle_1 \pm |b_1\rangle\,|v\rangle_1\right). \tag{7}$$

We can rewrite (5) by using these states as a basis:

$$\begin{aligned}\tfrac{1}{2}|c_+\rangle\left(\alpha|a_2\rangle + \beta|b_2\rangle\right)|h\rangle_2 + \tfrac{1}{2}|c_-\rangle\left(\alpha|a_2\rangle - \beta|b_2\rangle\right)|h\rangle_2 \\ + \tfrac{1}{2}|d_+\rangle\left(\beta|a_2\rangle + \alpha|b_2\rangle\right)|h\rangle_2 \\ + \tfrac{1}{2}|d_-\rangle\left(\beta|a_2\rangle - \alpha|b_2\rangle\right)|h\rangle_2\,.\end{aligned} \tag{8}$$

For Alice, it is simply a question of measuring on the basis $|c_\pm\rangle$, $|d_\pm\rangle$. To do this we first rotate the polarization of path b_1 by a further 90° (in the actual experiment this was done by setting the angle of the Fresnel rhomb in path b_1 at $\theta + 90°$ rather than by using a separate plate as shown

in the figure) so that the state $|b_1\rangle|v\rangle_1$ becomes $-|b_1\rangle|h\rangle_1$ and the state $|b_1\rangle|h\rangle_1$ becomes $|b_1\rangle|v\rangle_1$. Thus,

$$|c_\pm\rangle \rightarrow \frac{1}{\sqrt{2}}(|a_1\rangle \pm |b_1\rangle)|v\rangle_1\,, \tag{9}$$

$$|d_\pm\rangle \rightarrow \frac{1}{\sqrt{2}}(|a_1\rangle \mp |b_1\rangle)|h\rangle_1\,. \tag{10}$$

Paths a_1 and b_1 now impinge on the two input ports of an ordinary 50:50 beam splitter (BS). At this BS each of the two polarizations h and v interfere independently. After BS, there are two sets of detectors $D_{A_\pm}$ and $D^\perp_{A_\pm}$ which are coupled, respectively, to the h and v polarizations, being the ones selected by two polarizing beam splitters (PBS). A click registered at $D^\perp_{A_\pm}$ corresponds to a measurement onto $|c_\pm\rangle$ while a click registered at $D_{A_\pm}$ corresponds to a measurement onto $|d_\mp\rangle$. Furthermore, the position Δz of BS is set in such a way that the detectors D_{A_+} and $D^\perp_{A_+}$ are excited by the photon in the state $\frac{1}{\sqrt{2}}(|a_1\rangle + |b_1\rangle)$ while D_{A_-} and $D^\perp_{A_-}$ are excited by state $\frac{1}{\sqrt{2}}(|a_1\rangle - |b_1\rangle)$. In this way each of the four Bell states [(6) and (7)] can be measured.

The paths a_2 and b_2, taken by the photon sent to Bob, originate from backreflections at the end of the two calcite crystals and are transmitted through the BBO crystal. The path a_2 is rotated through 90° by a half-wave plate and is combined with b_2 at a polarizing beamsplitter (PBS_B) oriented to transmit horizontal and to reflect vertical polarizations. The state in (8) becomes

$$\begin{aligned}&\tfrac{1}{2}|c_+\rangle(\beta|h\rangle_2 + \alpha|v\rangle_2) + \tfrac{1}{2}|c_-\rangle(-\beta|h\rangle_2 + \alpha|v\rangle_2)\\ &\quad + \tfrac{1}{2}|d_+\rangle(\alpha|h\rangle_2 + \beta|v\rangle_2)\\ &\quad + \tfrac{1}{2}|d_-\rangle(-\alpha|h\rangle_2 + \beta|v\rangle_2)\,.\end{aligned} \tag{11}$$

Bob's photon can be transformed back to the original state $\alpha|v\rangle + \beta|h\rangle$ by applying an appropriate unitary transformation, depending on the outcome of Alice's measurement. However, we are simply interested in verifying that the appropriate state has been produced at Bob's end so, rather than performing these unitary transformations, we will simply orient (by acting on a polarization rotator R_B and on a quarter-wave plate) the measuring apparatus at end 2 appropriately for each of Alice's outcomes (the transformations can either be seen as *active* transformations or as a *passive* reorientation of our reference system, with respect to which the verification measurements are made). In the case of linear polarization the verification measurements can be accomplished by rotating the polarization of the state through an angle θ_B by means of a Fresnel rhomb device (R_B), then letting it impinge on a polarizing beam splitter followed by two detectors $D(\theta_B)$ (a photon originally incident with polarization θ_B would certainly be detected at this detector) and $D(\theta_B^\perp)$. In the more general case of elliptical polarization we can add, before R_B, a quarter-wave plate oriented at an angle γ_B with respect to the horizontal direction.

Wide filters ($\Delta\lambda = 20$ nm) were placed just before each detector. Wide, rather than narrow, filters were used so that the count rate was high enough to allow measurements to be made in a few seconds in order that problems associated with phase drift were minimized.

The beam splitter and the back reflecting mirror acting on path b_2 were each mounted on a computer controlled micrometrical stage which could be incremented in 0.1 μm steps. To align the system, a half-wave plate oriented at 45° to the vertical was placed before one of the calcite crystals to rotate the polarization by 90°. This had the effect of sending both photons to Alice's end or Bob's end. The correct values of Δz and Δy were found by looking for an interference dip in the coincidence count rates between D_{A_+} and D_{A_-} at Alice's end, and between D(45°) and D(−45°) at Bob's end. After alignment, the half-wave plate was rotated 0° to the vertical so that it had no effect on the polarization of photons passing through it. The distance between the Alice's and Bob's apparatuses was about 2.5 m. The coincidence time window was 1.6 ns and each measurement was taken over runs lasting 10 s. Typically, there were about 5×10^2 coincidence counts during each run.

We will report separately on two aspects of the experiment. First, using three equally spaced linear polarization settings (0°, +120°, −120°), we will see that the classical teleportation limit in Eq. (3) is surpassed. Second we will see that, for some arbitrary states (linear and elliptically polarized), we see all of the expected features.

Let $I(\theta_B)$ be the coincidence count between $D(\theta_B)$ and one of Alice's detectors. Let $I_\parallel$ be the coincidence rate when θ_B is oriented so as to measure the projection operator onto the corresponding term in (11). For example, if $\theta = 120°$, then Alice's output $|d_+\rangle$ corresponds to $\theta_B = -30°$. (In the present work all polarization angles are referred to the horizontal direction.) Let $I_\perp$ be the count rate when θ_B is rotated through 90° from the value used to measure $I_\parallel$. We will have $I_\parallel = k|\langle\phi|\phi_{\text{tele}}\rangle|^2$ and $I_\perp = k|\langle\phi_\perp|\phi_{\text{tele}}\rangle|^2$, where $|\phi\rangle$ is the prepared state and $|\phi_{\text{tele}}\rangle$ is the state that is actually produced at Bob's side by the teleportation process. If the state produced at Bob's end is not pure then this analysis is easily adapted by summing over a particular decomposition of the impure state. The normalization constant k depends on the detector efficiencies. Since $I_\parallel + I_\perp = k$, we show that $|\langle\phi|\phi_{\text{tele}}\rangle|^2 = I_\parallel/(I_\parallel + I_\perp)$. To beat the classical teleportation limit the average value of this quantity must exceed $\frac{3}{4}$. This average is taken over three equally spaced linear polarizations (each weighted with probability $\frac{1}{3}$) and over each of the four possible outcomes of Alice's Bell state measurement (each weighted by $\frac{1}{4}$). With the average understood to be in this sense we can write $S = [I_\parallel/(I_\parallel + I_\perp)]_{\text{av}}$. This quantity was measured, and we found that $S = 0.853 \pm 0.012$. This represents a violation of the

classical teleportation limit by eight standard deviations. Note, if $I_{\parallel} = I_{\max}$ and $I_{\perp} = I_{\min}$ (as we would expect, and as is indeed true for the data to be discussed below), and if the quantity in (12) is greater than $\frac{3}{4}$, then the visibility is greater than 50% (and vice versa).

Now consider in more detail one linear polarization case. All of the quarter-wave plates were removed in this case. In Fig. 2, we show the count rates related to four *simultaneous* coincidence experiments between each outcome of Alice's Bell state measurement ($c_{\pm}$ and $d_{\pm}$) and Bob's detector $D(\theta_B)$ as a function of θ_B for the particular case where the preparer prepared linear polarization with $\theta = 22.5°$. Note that the displacements of the maxima are 22.5°, 67.5°, −67.5°, and −22.5°. These are consistent with Eq. (11), where $\alpha = \sin(\theta)$ and $\beta = \cos(\theta)$. In the present experiment the detector $D(\theta_B^{\perp})$ is used only for the alignment of Bob's apparatus.

To prepare an elliptical polarized state we set $\theta = 0°$ and insert the quarter-wave plates at angle γ equal to 20°. This produced the elliptically polarized state,

$$\frac{1}{\sqrt{2}}[(1 + i\cos(2\gamma))\,|v\rangle + \sin(2\gamma)\,|h\rangle]. \qquad (12)$$

To verify that the state had been teleported according to Eq. (11) a quarter-wave plate was used at Bob's end, oriented at angle γ_B. A different setting of this was used corresponding to each of Alice's outcomes. For outcomes $|d_{\pm}\rangle$ we set $\gamma_B = \pm\gamma + 90°$. This converts the corresponding state at Bob's side to $|v\rangle$. For outcomes $|c_{\pm}\rangle$ we set $\gamma_B = \pm\gamma$. This converts the corresponding state at Bob's side to $|h\rangle$. The state was then analyzed in linear polarization over a range of values of θ_B. The results, shown in Fig. 3, demonstrate that the state after the quarter-wave plate is vertically or horizontally polarized, as required.

In this paper we have seen how a state, which is totally unknown to Alice, can be disassembled into purely classical and purely nonlocal EPR correlations and then reconstructed at a distant location. In the reconstruction procedure we took an essentially passive view of the unitary transformations. Work is currently in progress to implement the transformations in an active way by using fast Pockels cells fired by Alice's detectors.

We thank G. Di Giuseppe, V. Mussi, and D. P. Di Vincenzo for discussions, and the CEE-TMR (Contract No. ERBFMRXCT96-066) and INFM (Contract No. PRA97-cat) for funding. L. H. thanks the Royal

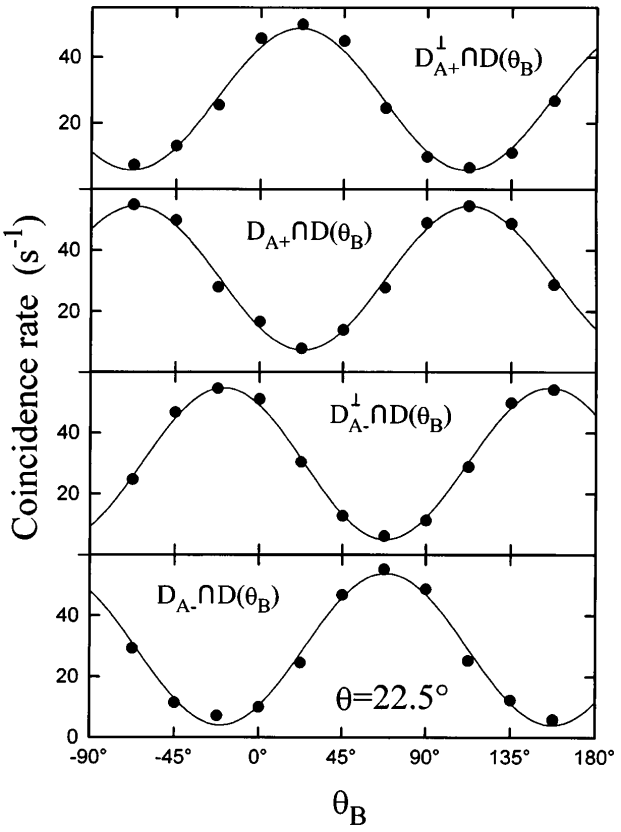

FIG. 2. Results for a linear polarized state at 22.5° to the horizontal obtained by four *simultaneous* coincidence experiments involving the four detectors D_A at Alice's site and Bob's detector $D(\theta_B)$. The graphs show the coincidence rates as a function of the angle θ_B. The error bars are smaller than the dots.

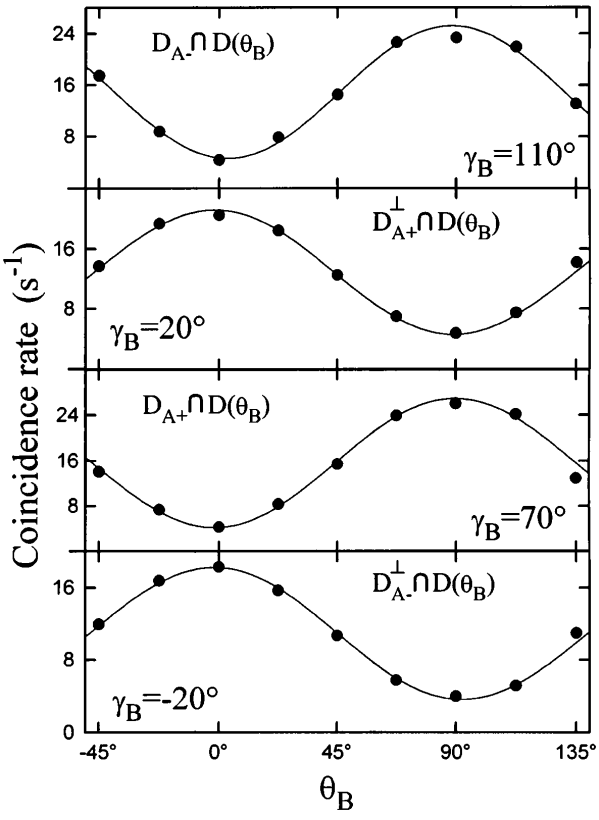

FIG. 3. Results of four coincidence experiments the same as for Fig. 2 but for an elliptically polarized case generated by using a quarter-wave plate at angle 20° with respect to the horizontal.

Society for support. The present work originates from a lecture delivered by S. P. and attended by F. D. M. in July, 1995, at the annual meeting on Quantum Computation in Torino, Italy. We thank the organizers of that meeting: the I.S.I. Foundation and ELSAG-BAILEY.

Appendix.—Define the normalized state $|\Omega_l\rangle$ by $|\varepsilon_l\rangle = \sqrt{\mu_l}\,|\Omega_l\rangle$ where $\mu_l = \langle\varepsilon_l|\varepsilon_l\rangle$. By taking the trace of (1), we obtain $\sum_l \mu_l = 2$. The 2 here corresponds to the dimension of the Hilbert space. Define $T_l = \sum_a |\langle\phi_a|\phi_l^c\rangle|^2 |\langle\phi_a|\Omega_l\rangle|^2$. Then $S = \sum_l \frac{1}{3}\mu_l T_l$. By varying with respect to the vectors $|\phi_l^c\rangle$ and $|\Omega_l\rangle$ we obtain $T_l^{\max} = \frac{9}{8}$. Hence, $S \leq \frac{3}{8}\sum_l \mu_l = \frac{3}{4}$. We obtain (3) as required.

[1] C. Bennett, G. Brassard, C. Crepeau, R. Jozsa, A. Peres, and W. Wootters, Phys. Rev. Lett. **70**, 1895 (1993).

[2] S. Popescu (to be published).

[3] The idea of using two degrees of freedom of a single photon rather than two photons was also considered, for other purposes, by M. Żukowski [Phys. Lett. A **157**, 198 (1991)].

[4] The "swap" operation is defined in a standard base $|i\rangle|j\rangle$ as $|i\rangle|j\rangle \rightarrow |j\rangle|i\rangle$ for all i, j which leads to $|\Psi\rangle|\Phi\rangle \rightarrow |\Phi\rangle|\Psi\rangle$ for any two arbitrary states.

[5] H. Weinfurter, Europhys. Lett. **25**, 559 (1994); S. L. Braunstein and A. Mann, Phys. Rev. A **51**, R1727 (1995); K. Mattle, H. Weinfurter, P. G. Kwiat, and A. Zeilinger, Phys. Rev. Lett. **76**, 4656 (1996).

[6] A. Peres, *Quantum Theory, Concepts, and Methods* (Kluwer, Dordrecht, 1993).

[7] For a uniform distribution of states over the Poincaré sphere, a lower upper bound is given in S. Massar and S. Popescu, Phys. Rev. Lett. **74**, 1259 (1995).

[8] D. Klyshko, *Photons and Nonlinear Optics* (Gordon and Breach, New York, 1988).

[9] P. G. Kwiat, K. Mattle, H. Weinfurter, A. Zeilinger, A. V. Sergienko, and Y. H. Shih, Phys. Rev. Lett. **75**, 4337 (1995); D. Boschi, Laurea thesis, Università di Roma "La Sapienza," 1995.

Unconditional Quantum Teleportation

A. Furusawa, J. L. Sørensen, S. L. Braunstein, C. A. Fuchs, H. J. Kimble,* E. S. Polzik

Quantum teleportation of optical coherent states was demonstrated experimentally using squeezed-state entanglement. The quantum nature of the achieved teleportation was verified by the experimentally determined fidelity $F^{exp} = 0.58 \pm 0.02$, which describes the match between input and output states. A fidelity greater than 0.5 is not possible for coherent states without the use of entanglement. This is the first realization of unconditional quantum teleportation where every state entering the device is actually teleported.

Quantum teleportation is the disembodied transport of an unknown quantum state from one place to another (*1*). All protocols for accomplishing such transport require nonlocal correlations, or entanglement, between systems shared by the sender and receiver. John Bell's famous theorem on the incompatibility of quantum mechanics with local hidden variable theories establishes that entanglement represents the quintessential distinction between classical and quantum physics (*2*). Recent advances in the burgeoning field of quantum information have shown that entanglement is also a valuable resource that can be exploited to perform otherwise impossible tasks, of which quantum teleportation is the prime example.

Teleportation of continuous quantum variables. To date, most attention has focused on teleporting the states of finite-dimensional systems, such as the two polarizations of a photon or the discrete level structure of an atom (*1, 3–8*). However, quantum teleportation is also possible for continuous variables corresponding to states of infinite-dimensional systems (*9, 10*), such as optical fields or the motion of massive particles (*11*). The particular implementation of teleported optical fields is noteworthy in four ways. First, the relevant optical tools are powerful and well suited for integration into an evolving communication technology. Second, these methods apply to other quantum computational protocols, such as quantum error correction for continuous variables using linear optics (*12*) and superdense coding of optical information (*13*). Third, finite-dimensional systems can always be considered as subsystems of infinite-dimensional systems where the above advantages can be put to use. Finally, a relatively simple design is implemented that eliminates the need for some nonlinear operations (*10*); these nonlinear operations constitute the main bottleneck to the efficacy of other teleportation schemes.

This teleportation scheme uses the protocol described in (*10*). The experimental setup (Fig. 1) consists of a sending station operated by Alice, a receiving station operated by Bob, and a station for producing beams of entangled photons [labeled EPR (Einstein-Podolsky-Rosen) beams (1, 2)]. Alice and Bob each receive half of the EPR photons. Alice's station consists of two homodyne detectors $D_{x,p}$ (including two local oscillators $LO_{x,p}$), where x and p denote the real and imaginary components of the (complex) electric field. These detectors measure an entangled combination of the input state $|v_{in}\rangle$ and Alice's half of the EPR beam. Classical lines of communication are used to transmit Alice's measurement results to Bob, who then uses that information to transform the second half of the EPR beam (at the mirror m_{Bob}) into an output $\hat{\rho}_{out}$ that closely mimics the original unknown input.

In our scheme, a third party, Victor (the verifier), prepares an initial input in the form of a coherent state of the electromagnetic field $|v_{in}\rangle$, which he then passes to Alice for teleportation. Likewise, the teleported field that emerges from Bob's sending station is interrogated by Victor to verify that teleportation has actually taken place: At this stage, Victor records the amplitude and variance of the field generated by Bob, and is thereby able to assess the "quality" of the teleportation protocol. This is done by determining the overlap between input and output as given by the fidelity $F \equiv \langle v_{in}|\hat{\rho}_{out}|v_{in}\rangle$. As discussed below, for the teleportation of coherent states, $F_c = 0.5$ sets a boundary for entrance into the quantum domain in the sense that Alice and Bob can exceed this value only by making use of entanglement (*14*). From Victor's measurements of orthogonal quadratures (see below), our experiment achieves $F^{exp} = 0.58 \pm 0.02$ for the field emerging from Bob's station, thus demonstrating the nonclassical character of this experimental implementation.

To describe the infinite-dimensional states of optical fields, it is convenient to introduce a pair (x, p) of continuous variables of the electric field, called the quadrature-phase amplitudes (QAs), that are analogous to the canonically conjugate variables of position and momentum of a massive particle (*15*). In terms of this analogy, the entangled beams shared by Alice and Bob have nonlocal correlations similar to those first described by Einstein *et al*. (*16*). The requisite EPR state is efficiently generated via the nonlinear optical process of parametric down-conversion previously demonstrated in (*17*). The resulting state corresponds to a squeezed two-mode optical field. In the ideal case, namely perfect EPR correlations and lossless propagation and detection, the teleported state emerges from Bob's station with perfect fidelity $F = 1$ (*10*).

Apart from the advantages of continuous quantum variables, our experiment is significant in that it attains full teleportation as originally envisioned in (*1*). This is in contrast to previous teleportation experiments where no physical state enters the device from the outside (*7*) or where the teleported state is destroyed at Bob's station (*8*), never emerging for subsequent exploitation (*18*). Furthermore, in both these previous experiments, there never exists an actual physical field with high (nonclassical) teleportation fidelity at the output.

Apparatus and protocol. As illustrated in Fig. 1, entangled EPR beams are generated along paths {1, 2} by combining two independent squeezed beams at a 50/50 beam splitter (*19*), with the relative phase between the squeezed fields actively servo-controlled. The squeezed fields are themselves produced by parametric down-conversion in a subthreshold optical parametric oscillator (OPO) (*20*). The particular setup is as described in (*21*), save one important exception. Because the cavity for the OPO is a traveling-wave resonator (that is, a folded-ring geometry), it is possible to drive the intracavity nonlinear crystal with two counterpropagating pump beams to generate two (nominally) independent squeezed fields countercirculating within the cavity and emerging along the separate paths {*i*, *ii*} (see Fig. 1). Note that the light from a single-frequency titanium sapphire ($TiAl_2O_3$) laser at 860 nm serves as the primary source for all fields in our experiment. Ninety percent of the laser output at frequency ω_L is directed to a frequency-doubling cavity to generate roughly 300 mW of blue light at $2\omega_L$ (*22*), with this output then split into two beams that serve as harmonic pumps for (degenerate) parametric down-conversion, $2\omega_L \rightarrow \omega_L \pm \Omega$, within the OPO. Both

A. Furusawa, C. A. Fuchs, H. J. Kimble are in the Norman Bridge Laboratory of Physics, California Institute of Technology, Pasadena, CA 91125, USA. J. L. Sørensen and E. S. Polzik are at the Institute of Physics and Astronomy, Aarhus University, Aarhus 8000, Denmark. S. L. Braunstein is at the School of Electrical Engineering and Computer Systems, University of Wales, Bangor LL57 1UT, UK.

*To whom correspondence should be addressed. E-mail: hjkimble@cco.caltech.edu

the doubling cavity and the cavity of the OPO contain an *a*-cut potassium niobate ($KNbO_3$) crystal for temperature-tuned, noncritical phase matching, with the lengths of both cavities under servo-control to maintain resonance for a TEM_{00} longitudinal mode.

Our protocol is as follows: EPR beam 1 (Fig. 1) propagates to Alice's sending station, where it is combined at a 50/50 beam splitter with the unknown input state $|v_{in}\rangle$, which is a coherent state of complex amplitude $v_{in} \equiv x_{in} + ip_{in}$. Alice uses two sets of balanced homodyne detectors (D_x, D_p) to make a "Bell-state" measurement of the amplitudes $x = (x_{in} - x_1)/\sqrt{2}$ and $p = (p_{in} + p_1)/\sqrt{2}$ for the input state and the EPR field 1 of amplitude $\alpha_1 \equiv x_1 + ip_1$. The classical (photocurrent) outcomes are denoted by (i_x, i_p) respectively, and are scaled to (x, p). At unit efficiency, such detectors provide "optimal" information about (x, p) via (i_x, i_p) (*23–25*), with the knowledge gained about the unknown input state $|v_{in}\rangle$ going to zero as $\sigma^{-}_{i,ii} \rightarrow 0$, where $\sigma^{-}_{i,ii}$ denotes the variances of squeezed QAs of the fields along paths {i, ii}.

Because of the entanglement between the EPR beams {1, 2}, Alice's Bell-state detection collapses Bob's field 2 into a state conditioned on the measurement outcome (i_x, i_p). Hence, after receiving this classical information from Alice, Bob is able to construct the teleported state $\hat{\rho}_{out}$ via a simple phase-space displacement of the EPR field 2 (*26*). In our experiment, the amplitude and phase modulators (M_x, M_p) shown in Fig. 1 transform the (amplified) photocurrents (i_x, i_p) into a complex field amplitude, which is then combined with the EPR beam 2 at the mirror m_{Bob} of reflectivity 0.99. In this manner, we affect the displacement $\alpha_2 \rightarrow v_{out} = \alpha_2 + g\sqrt{2}(i_x + ii_p) = gv_{in} + [(x_2 - gx_1) + i(p_2 + gp_1)]$, where g describes Bob's (suitably normalized) gain for the transformation from photocurrent to output field. In the limit $\sigma^{-}_{i,ii} \rightarrow 0$, $(x_1 - x_2, p_1 + p_2) \rightarrow 0$ [that is, the EPR beams become "quantum copies" of each other with respect to their QAs (*19*)], so that for $g = 1$, $\hat{\rho}_{out} \rightarrow |v_{in}\rangle\langle v_{in}|$, resulting in perfect teleportation with fidelity $F \rightarrow 1$.

Quantum versus classical teleportation. Of course, the limit $F = 1$ is reached only for ideal (singular) EPR correlations and for lossless propagation and detection. To aid in quantifying the "quality" of teleportation in our actual experiment, we calculate F for the case of a finite degree of EPR correlation and in the presence of non-unit efficiencies, which for a coherent-state input $|v_{in}\rangle$ becomes

$$F = 2/\sigma_Q \exp[-2|v_{in}|^2(1-g)^2/\sigma_Q] \quad (2)$$

(*14*), where σ_Q is the variance of the Q function of the teleported field, given by

$$\sigma_Q = 1 + g^2 + (\sigma^{-}/2)(g\xi_1 + \xi_2)^2 + (\sigma^{+}/2)(g\xi_1 - \xi_2)^2 + (1 - \xi_1^2)g^2 + (1 - \xi_2^2) + 2g^2(1/\eta^2) - 1) \quad (2)$$

Here, $\sigma^{\pm}$ are the variances of the amplified/squeezed QAs that are summed to form the EPR beams (assuming $\sigma^{\pm}_i = \sigma^{\pm}_{ii}$), $\xi_{1,2}$ characterize the (amplitude) efficiency with which the EPR beams are propagated and detected along paths {1, 2}, and η gives the (amplitude) efficiency for detection of the unknown input state by Alice (*10*).

Classical teleportation replaces the EPR beams by (uncorrelated) vacuum inputs ($\sigma^{\pm} \rightarrow 1$), thus eliminating the shared entanglement between Alice and Bob. For coherent states distributed across the complex plane, optimum fidelity is achieved for $g \approx 1$, in which case $(\sigma_Q - 1) = \sigma_W \geq 3$ and $F \leq 0.5$, and equality is obtained only for $\eta = 1$. In this case, one unit of vacuum noise in the variance σ_W of the Wigner distribution arises from the original coherent-state input ($\sigma_{in} = 1$), whereas the other two units are the so-called quantum duties (or quduties) that must be paid at each crossing of the border between quantum and classical domains (*10*). One quduty arises from Alice's attempt to infer both QAs of the field (*23*); the other quduty results from Bob's displacement.

However, quantum teleportation should necessarily require Alice and Bob to share a nonlocal quantum resource, such as the EPR beams in our experiment. The question of the operational verification of this shared entanglement is relevant not only to our teleportation protocol, but also to eavesdropping in quantum cryptography (*27*). So long as Alice and Bob can communicate only over a classical channel, we have shown that for $g = 1$, $\sigma_W > \sigma_{in} + 2$, so that $\sigma^{c}_W = 3$ heralds the boundary between quantum and classical teleportation for coherent-state inputs. More generally, even in the absence of loss, Alice and Bob can achieve $F > 1/2$ for an unknown coherent state only by way of shared quantum entanglement, as can be operationally (and independently) verified by Victor (*14*). Note that for experiments involving photon polarization as in (*7, 8*), the corresponding fidelity threshold for a completely unknown quantum state is $F > 2/3$ (*28*), which could not be approached because of the low detection efficiencies. Moreover, in contrast to the work in (*7, 8*), Victor need not to make any arrangement with Alice and Bob in order to make an objective assessment of the quantum nature of the teleportation process.

Experimental results. We concentrate first on Alice's measurement of the unknown input state (Fig. 2). The spectral density of photocurrent fluctuations $\Psi_x^{Alice}(\Omega)$, recorded by Alice's balanced homodyne detector D_x as the phase ϕ_{in} of the coherent-state input [$v_{in} = |v_{in}|\exp(i\phi_{in})$] is swept linearly by Victor, is shown in Fig. 2A. For $\phi_{in} - \theta_{A,x} = p\pi$ (with integral p and $\theta_{A,x}$ as the phase of local oscillator at D_x), $\Psi_x^{Alice}(\Omega)$ rises to a maximum, while for half-integral p it falls to a minimum that is set by the variance of EPR beam 1. A completely analogous set of traces is obtained for the output from Alice's detector D_p, except now shifted in phase by $\pi/2$ in correspondence to the fact that phases of the local oscillator beams at (D_x, D_p) are fixed to be in quadrature by active servo-control. For $v_{in} = 0$, the phase-insensitive noise levels shown in Fig. 2A correspond to the case of no EPR beams present [that is, $\sigma^{\pm}_{i,ii} \rightarrow 1$, giving the vacuum-state level $\Phi_{0,x}^{Alice}(\Omega)$] and to that with the EPR beam 1 distributed to Alice [excess noise at the level $\Lambda_x^{Alice}(\Omega)$]. A more detailed view of these noise levels is provided in Fig. 2B. The observed increases in photocurrent fluctuations from $\Phi_{0,(x,p)}^{Alice} \rightarrow \Lambda_{(x,p)}^{Alice}$ represent the necessary degradation in signal-to-noise ratio for Alice that accompanies quantum teleportation, with $\Lambda_{(x,p)}^{Alice} \rightarrow \infty$ in the

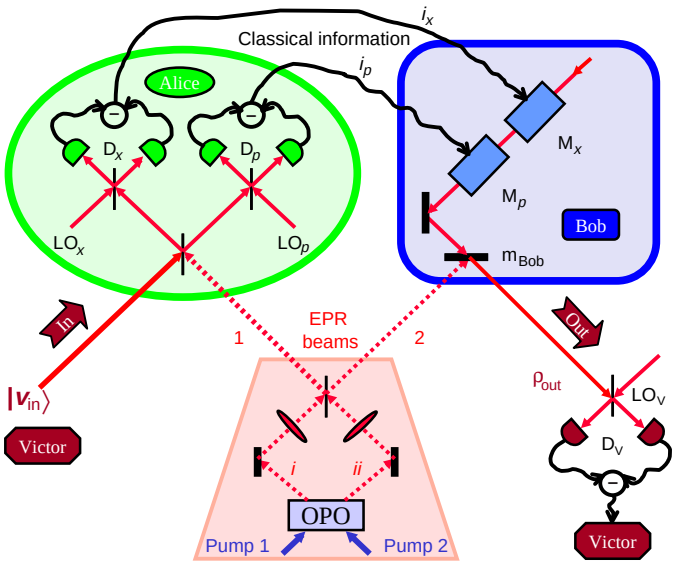

Fig. 1. Schematic of the experimental apparatus for teleportation of an unknown quantum state $|v_{in}\rangle$ from Alice's sending station to Bob's receiving terminal by way of the classical information (i_x, i_p) sent from Alice to Bob and the shared entanglement of the EPR beams (1, 2).

limit of perfect teleportation (for which $\sigma^{-}_{i,ii} \rightarrow 0$, $\sigma^{+}_{i,ii} \rightarrow \infty$, and hence the variance σ_1 of the EPR beam 1 diverges).

The various spectral densities displayed in Fig. 2 are directly related to the means and variances of the quadrature-phase amplitudes of the incident fields (*17, 19*). Because we are dealing with broad-bandwidth fields, the single-mode treatment of (*10*) must be generalized to the case of multimode fields of finite bandwidth (*29*). In this situation, the relevant quantities are the spectral components ($x(\Omega)$, $p(\Omega)$) of the QAs, where a general QA at phase δ is defined by

$$z(\Omega,\delta) \equiv \int_{\Omega-\Delta\Omega}^{\Omega+\Delta\Omega} d\Omega' [\hat{a}(\Omega') \exp(-i\delta) + \hat{a}^{\dagger}(-\Omega') \exp(+i\delta)] \quad (3)$$

with $\hat{a}(\hat{a}^{\dagger})$ as the annihilation (creation) operator for the field at offset Ω from the optical carrier, with $(x(\Omega), p(\Omega)) = (z(\Omega, 0), z(\Omega, \pi/2))$, and with the integration extending over a small interval ΔΩ about Ω. We then have

$$\Psi(\Omega)\Delta\Omega \sim \langle z^2(\Omega,\delta)\rangle \quad (4)$$

(*15, 17*). As shown in (*29*), the teleportation protocol of (*10*) remains unchanged in its essential character. However, now the state being teleported describes the field at frequency offset $\pm\Omega$ within a bandwidth ΔΩ about the carrier ω_L (that is, AM and FM modulation sidebands), with FM sidebands applied by Victor to create the input $v_{in}(\Omega)$.

Given Alice's measurement of $(x(\Omega), p(\Omega))$, the next step in the protocol is for her to send the (classical) photocurrents $(i_x(\Omega), i_p(\Omega))$ to Bob, who uses this information to generate a displacement (a coherent modulation at Ω) of the field in beam 2 by way of the modulators (M_x, M_p) and the mirror m_{Bob}. Note that the phases of both Alice's and Bob's fields relative to the EPR beams {1, 2} are fixed by servo-control. Bob's action results in the teleported output field, which is subsequently interrogated by Victor by way of his own (independent) balanced homodyne detector. Shown in Fig. 3 is Victor's measurement of the QAs of the teleported field, as expressed by the spectral density of photocurrent fluctuations $\Psi^{Victor}(\Omega)$ as a function of time, again as the phase ϕ_{in} is linearly swept. Here, the gain is $g = 1$ (that is, 0 dB), so that Victor's signal level rises 3 dB above that in Fig. 2A, in correspondence to a reconstruction of the coherent amplitude $v_{in}(\Omega) \rightarrow v_{out}(\Omega)$ for the output field. This transformation is independent of the phase of the input field relative to Alice's detectors (D_x, D_p) and to the consequent division of this amplitude to Bob's modulators (M_x, M_p), so that the phase of the teleported field tracks that of the input. In the particular case of Fig. 3A, the phase ϕ_{Victor} of Victor's local oscillator is servo-controlled relative to Alice's and Bob's fields, but it can as well be freely scanned. As in Fig. 2, the phase-insensitive noise levels in Fig. 3A correspond to the case of a vacuum-state input $v_{in} = 0$, first with no EPR beams present (that is, classical teleportation with $\sigma^{\pm}_{i,ii} \rightarrow 1$), giving the level $Y_0^{Victor}(\Omega)$, and then to quantum teleportation with the EPR beams {1, 2} distributed to Alice and Bob, giving $\Lambda^{Victor}(\Omega)$. These noise levels are shown in somewhat more detail in Fig. 3B.

For $g = 1$ (0 dB), as here, the level Y_0^{Victor} stands ~4.8 dB above Victor's vacuum-state level Φ_0^{Victor}, in correspondence to the three units of vacuum noise previously discussed. However, in contradistinction to the increases $\Phi^{Alice}_{0,(x,p)} \rightarrow \Lambda^{Alice}_{(x,p)}$ recorded by Alice, Victor observes a decrease in fluctuations $Y_0^{Victor} \rightarrow \Lambda^{Victor}$ brought about by the presence of the EPR beams, indicating the success of the teleportation protocol. More quantitatively, for $g = 1$, Victor observes a decrease of $10[\log \Lambda^{Victor}(\Omega) - \log Y_0^{Victor}(\Omega)] = -1.2 \pm 0.2$ dB. The ratio $\Lambda^{Victor}(\Omega)/\Phi_0^{Victor}(\Omega)$ then leads directly to the variance $\sigma_W = 2.23 \pm 0.03 < \sigma^c_W = 3$ for the teleported field.

Demonstration of quantum teleportation. By carrying out a series of measurements similar to those shown in Figs. 2 and 3, we have explored the dependence of both the variance of the teleported field and the fidelity F on Bob's gain g. Plotted in Fig. 4 as a function of g are the variances $\sigma^{x,p}_W$ obtained by Victor at D_V for

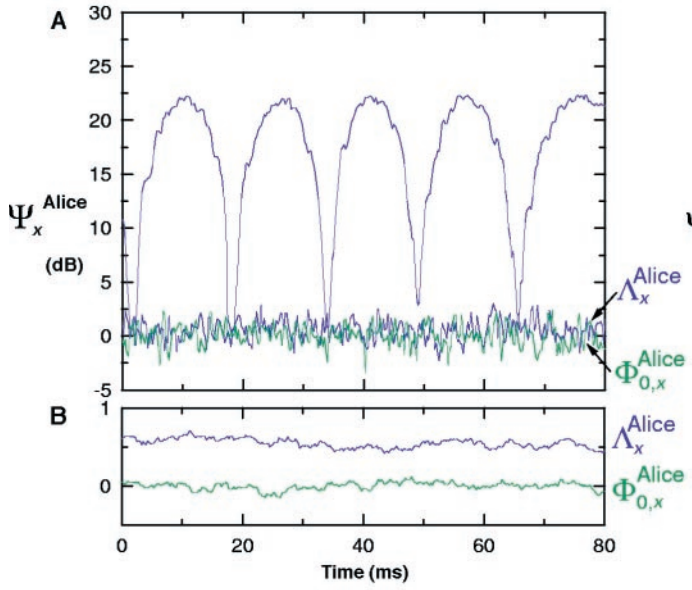

Fig. 2 (left). (**A**) Spectral density of photocurrent fluctuations $\Psi_x^{Alice}(\Omega)$ recorded by Alice's balanced homodyne detector D_x as a function of time with the phase ϕ_{in} of the coherent-state input linearly swept. For the case of a vacuum-state input $v_{in} = 0$ and with no EPR beams present, the vacuum-state level $\Phi_{0,x}^{Alice}(\Omega)$ results, whereas with $v_{in} = 0$ and EPR beam 1 distributed to Alice, excess noise at the level $\Lambda_x^{Alice}(\Omega)$ is recorded. (**B**) Expanded view for $v_{in} = 0$, now with a 10-trace average. Acquisition parameters: radio frequency (rf) $\Omega/2\pi = 2.9$ MHz, rf bandwidth $\Delta\Omega/2\pi = 30$ kHz, video bandwidth = 1 kHz (A) and 30 Hz (B).

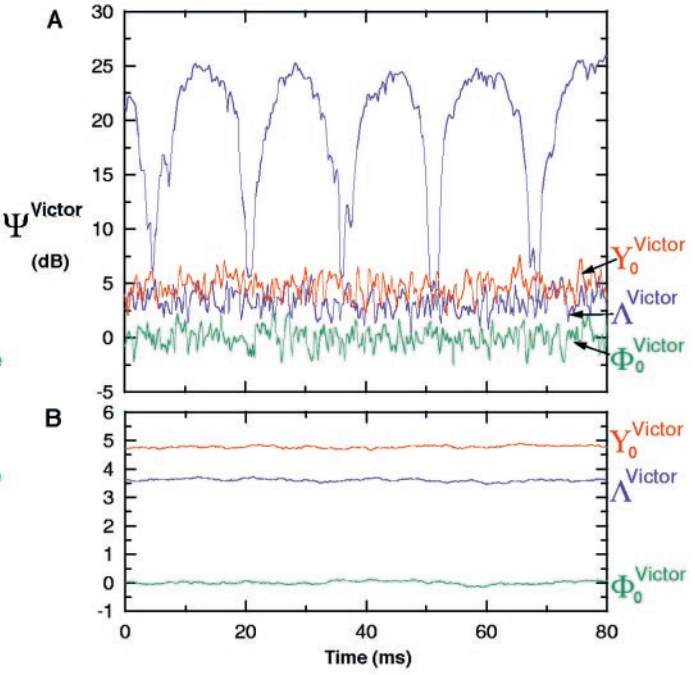

Fig. 3 (right). (**A**) Spectral density of photocurrent fluctuations $\Psi^{Victor}(\Omega)$ recorded by Victor's balanced homodyne detector D_V as afunction of time with the phase ϕ_{in} of the coherent-state input linearly swept and with the gain $g \approx 1$. For the case of a vacuum-state input $v_{in} = 0$ and with no EPR beams present, the excess noise level $Y_0^{Victor}(\Omega)$ results, whereas with $v_{in} = 0$ and EPR beams {1, 2} distributed to Alice and Bob, the level of fluctuations is reduced to $\Lambda^{Victor}(\Omega)$. The vacuum-state level for D_V is given by Φ_0^{Victor}. (**B**) Expanded view for $v_{in} = 0$, now with a 10-trace average. Acquisition parameters are as in Fig. 2.

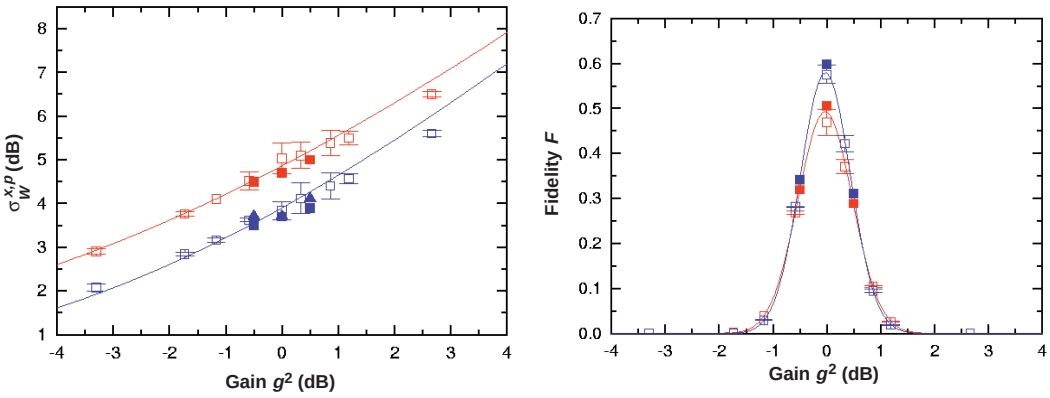

Fig. 4 (left). Variance $\sigma_W^{x,p}$ of the teleported field measured by Victor as a function of the gain g used by Bob for the phase-space displacement of the EPR beam 2. Shown are data obtained both with the quantum-correlated EPR beams present (blue) and with vacuum-state inputs (red) for beams {1, 2}. Open and filled symbols represent results of two different experiments. The theoretical results from Eq. 2 (curves) are also shown for the two cases of quantum and classical teleportation. **Fig. 5 (right).** Fidelity F inferred from measurements of the input amplitude v_{in} and of the quantities v_{out} and $\sigma_Q^{x,p}$ for the teleported output field. Data for the cases of classical (red) and quantum (blue) teleportation are shown, as are the theoretical results from Eq. 1 (curves). See text for explanations of filled and open symbols. $F > 0.5$ demonstrates the nonclassical nature of the protocol.

measurements with the phase ϕ_{Victor} locked to that of Alice's local oscillator at detector D_x (squares) and D_p (triangles), with the open and filled symbols from two different experiments. Comparison of the data in Fig. 4 with the theoretical result from Eq. 2 and the independently measured quantities $\xi_{1,2} = 0.90 \pm 0.04$, $\eta^2 = 0.97 \pm 0.02$, and $\{\sigma^- = 0.5 \pm 0.1, \sigma^+ = 1.8 \pm 0.2\}$ yields reasonable agreement. In particular, the EPR beams bring a reduction of $\sigma_W^{x,p}$ below the limit σ_W^c for classical teleportation with vacuum-state inputs over a reasonably wide range in g. Results similar to these are obtained for σ_W with ϕ_{Victor} swept independent of (D_x, D_p). Note that in a given experiment, we observe a systematic increase in $\sigma_W^p/\sigma_W^x \approx 1.05$, which is presumably associated with asymmetries and non-ideal couplings of the squeezed beams $\{i, ii\}$ that are summed to produce the EPR beams {1, 2} (*17*).

Data as in Fig. 4, together with a record of the mean coherent amplitude $\beta_{out}(\Omega) = g v_{in}(\Omega)$ measured by Victor for the teleported field, allow us to infer the fidelity by way of a simple generalization of Eq. 1, namely

$$F = \frac{2}{\sqrt{\sigma_Q^x \sigma_Q^p}} \exp\left(-2|v_{out} - v_{in}|^2 / \sqrt{\sigma_Q^x \sigma_Q^p}\right) \quad (5)$$

Here, $\sigma_Q^{x,p} \equiv (1 + \sigma_W^{x,p})$ are the variances for the Q function obtained by Victor from measurements of the spectral densities of photocurrent fluctuations (that is, without correction for his detection efficiencies). Again under the assumption of Gaussian statistics for the teleported field, we thus deduce F, with the results shown in Fig. 5. The filled points around $g = 1$ (0 dB) are from independent measurements of $\sigma_W^{x,p}$, whereas for the open symbols, we approximate $\sigma_W^p \approx 1.05\sigma_W^x$, as above. The theoretical curve is from Eq. 1 with the aforementioned values $\xi_{1,2}$, η, and $\sigma^{\pm}$. Although the agreement between theory and experiment is evidently quite reasonable, the essential observations are that (i) the fidelity for classical teleportation with $\sigma_{i,ii}^{\pm} = 1$ is found to be $F_c^{exp} = 0.48 \pm 0.03 < F_c$, and (ii) the fidelity for quantum teleportation is $F_q^{exp} = 0.58 \pm 0.02 > F_c$. Recall that $F_c = 0.5$ is the classical bound attainable by Alice and Bob in the absence of shared entanglement (*14*), so that $F_q^{exp} > F_c$ demonstrates the nonclassical nature of the experiment.

By exploiting squeezed-state entanglement, we have the first realization of quantum teleportation as originally proposed in (*1*): An unknown quantum state input to Alice's station is transported to a field recreated at Bob's remote station. The quantum nature of the protocol is demonstrated with reference to both the variance σ_W of the teleported field and its fidelity F relative to the original input state, where we emphasize that σ_W and F relate to a physical field emerging from Bob's station. Because we have made no correction for the finite efficiency of Victor's detection process, the fidelity of the actual teleported field is higher than that quoted. Even without such correction, the overall efficiency of our scheme, together with the shared entanglement of the EPR beams, ensure full quantum teleportation: A quantum state presented at the input is teleported with nonclassical fidelity on each and every trial (of duration given by the inverse bandwidth $1/\Delta\Omega$). This high-efficiency experimental implementation of a quantum algorithm for continuous variables suggests that other protocols, including quantum error correction (*12*) and superdense coding (*13*) of optical fields, are not far from realization.

References and Notes

1. C. H. Bennett *et al.*, *Phys. Rev. Lett.* **70**, 1895 (1993).
2. J. S. Bell, *Speakable and Unspeakable in Quantum Mechanics* (Cambridge Univ. Press, New York, 1988), p. 196.
3. L. Davidovich *et al.*, *Phys. Rev. A* **50**, R895 (1994).
4. J. I. Cirac and A. S. Parkins, *ibid.*, p. R4441.
5. T. Sleator and H. Weinfurter, *Ann. N.Y. Acad. Sci.* **755**, 715 (1995).
6. S. L. Braunstein and A. Mann, *Phys. Rev. A* **51**, R1727 (1995); *ibid.* **53**, 630 (1996).
7. D. Boschi *et al.*, *Phys. Rev. Lett.* **80**, 1121 (1998).
8. D. Bouwmeester *et al.*, *Nature* **390**, 575 (1997).
9. L. Vaidman, *Phys. Rev. A* **49**, 1473 (1994).
10. S. L. Braunstein and H. J. Kimble, *Phys. Rev. Lett.* **80**, 869 (1998).
11. B. Yurke, S. L. McCall, J. R. Klauder, *Phys. Rev. A* **33**, 4033 (1986).
12. S. L. Braunstein, *Nature* **394**, 47 (1998).
13. ——— and H. J. Kimble, in preparation.
14. S. L. Braunstein, C. A. Fuchs, H. J. Kimble, in preparation.
15. M. D. Reid and P. D. Drummond, *Phys. Rev. Lett.* **60**, 2731 (1988); M. D. Reid, *Phys. Rev. A* **40**, 913 (1989).
16. A. Einstein, B. Podolsky, N. Rosen, *Phys. Rev.* **47**, 777 (1935).
17. Z. Y. Ou, S. F. Pereira, H. J. Kimble, K. C. Peng, *Phys. Rev. Lett.* **68**, 3663(1992); Z. Y. Ou, S. F. Pereira, H. J. Kimble, *Appl. Phys. B* **55**, 265 (1992).
18. S. L. Braunstein and H. J. Kimble, *Nature* **394**, 840 (1998).
19. H. J. Kimble, in *Fundamental Systems in Quantum Optics, Les Houches, Session LIII, 1990*, J. Dalibard, J. M. Raimond, J. Zinn-Justin, Eds. (Elsevier, Amsterdam, 1992), pp. 549–674.
20. L. A. Wu *et al.*, *Phys. Rev. Lett.* **57**, 2520 (1986).
21. E. S. Polzik, J. Carri, H. J. Kimble, *ibid.* **68**, 3020 (1992); *Appl. Phys. B* **55**, 279 (1992).
22. E. S. Polzik and H. J. Kimble, *Opt. Lett.* **16**, 1400 (1991).
23. E. Arthurs and J. L. Kelly Jr., *Bell. Syst. Tech. J.* (April), 725 (1965).
24. H. P. Yuen and J. H. Shapiro, *IEEE Trans. Inf. Theory* **IT-26**, 78 (1980).
25. S. L. Braunstein, *Phys. Rev. A* **42**, 474 (1990).
26. Related work involves feedforward manipulation of twin-beam states [P. R. Tapster, J. G. Rarity, J. S. Satchell, *Phys. Rev. A* **37**, 2963 (1988); J. C. Mertz *et al.*, *Phys. Rev. Lett.* **64**, 2897 (1990)].
27. C. A. Fuchs and A. Peres, *Phys. Rev. A* **53**, 2038 (1996).
28. H. Barnum, thesis, University of New Mexico (1998).
29. P. van Loock, S. L. Braunstein, H. J. Kimble, in preparation.

30. The experiment was carried out in the Quantum Optics Group at the California Institute of Technology. Supported by the Quantum Information and Computation Institute funded by the Defense Advanced Research Projects Agency via the Army Research Office, by the Office of Naval Research, and by NSF. A.F. is a visiting scientist from the Nikon Research Laboratories. S.L.B. was funded in part by Engineering and Physical Sciences Research Council (UK) grant GR/L91344. C.A.F. also acknowledges support from a Lee A. DuBridge Fellowship. J.L.S. and E.S.P. acknowledge support from the Danish Research Council. We gratefully acknowledge the contributions of N. Ph. Georgiades and discussions with C. M. Caves, N. Cohen, S. J. van Enk, and H. Mabuchi.

20 July 1998; accepted 2 September 1998

7. Wootters, W. K. & Zurek, W. H. A single quantum cannot be cloned. *Nature* **299,** 802–803 (1982).
8. Nielsen, M. A. & Chuang, I. J. *Quantum Computation and Quantum Information* (Cambridge Univ. Press, Cambridge, 2000).
9. Gottesman, D. & Chuang, I. L. Demonstrating the viability of universal quantum computation using teleportation and single-qubit operations. *Nature* **402,** 390–393 (1999).
10. Furusawa, A. *et al.* Unconditional quantum teleportation. *Science* **282,** 706–709 (1998).
11. Nielsen, M. A., Knill, E. & Laflamme, R. Complete quantum teleportation using nuclear magnetic resonance. *Nature* **396,** 52–55 (1998).
12. Barrett, M. D. *et al.* Quantum teleportation with atomic qubits. *Nature* (this issue).
13. Schmidt-Kaler, F. *et al.* How to realize a universal quantum gate with trapped ions. *Appl. Phys. B* **77,** 789–796 (2003).
14. Roos, C. F. *et al.* Bell states of atoms with ultra long lifetimes and their tomographic state analysis. *Phys. Rev. Lett.* (in the press) Preprint at ⟨http://arXiv.org/abs/ physics/0307210⟩ (2003).
15. Massar, S. & Popescu, S. Optimal extraction of information from finite quantum ensembles. *Phys. Rev. Lett.* **74,** 1259–1263 (1995).
16. Gisin, N. Nonlocality criteria for quantum teleportation. *Phys. Lett. A* **210,** 157–159 (1996).
17. Kielpinski, D., Monroe, C. & Wineland, D. J. Architecture for a large-scale ion-trap quantum computer. *Nature* **417,** 709–711 (2002).
18. Gulde, S. *et al.* Implementation of the Deutsch-Jozsa algorithm on an ion-trap quantum computer. *Nature* **412,** 48–50 (2003).
19. Hahn, E. L. Spin Echoes. *Phys. Rev.* **80,** 580–594 (1950).

Acknowledgements We thank H. Briegel and P. Zoller for a critical reading of the manuscript. We gratefully acknowledge support by the Austrian Science Fund (FWF), by the European Commission (QUEST, QUBITS and QGATES networks), by the Institut für Quanteninformation, and by the Los Alamos LDRD Program. This material is based upon work supported in part by the US Army Research Office. H.H is funded by the Marie-Curie program of the European Union.

Competing interests statement The authors declare that they have no competing financial interests.

Correspondence and requests for materials should be addressed to R.B. (Rainer.Blatt@uibk.ac.at)

Deterministic quantum teleportation of atomic qubits

M. D. Barrett[1]*, J. Chiaverini[1], T. Schaetz[1], J. Britton[1], W. M. Itano[1], J. D. Jost[1], E. Knill[2], C. Langer[1], D. Leibfried[1], R. Ozeri[1] & D. J. Wineland[1]

[1]*Time and Frequency Division, NIST, Boulder, Colorado 80305, USA*
[2]*Mathematical and Computational Sciences Division, NIST, Boulder, Colorado 80305, USA*

* Present address: Department of Physics, University of Otago, PO Box 56, Dunedin, New Zealand

Quantum teleportation[1] provides a means to transport quantum information efficiently from one location to another, without the physical transfer of the associated quantum-information carrier. This is achieved by using the non-local correlations of previously distributed, entangled quantum bits (qubits). Teleportation is expected to play an integral role in quantum communication[2] and quantum computation[3]. Previous experimental demonstrations have been implemented with optical systems that used both discrete and continuous variables[4–9], and with liquid-state nuclear magnetic resonance[10]. Here we report unconditional teleportation[5] of massive particle qubits using atomic ($^9Be^+$) ions confined in a segmented ion trap, which aids individual qubit addressing. We achieve an average fidelity of 78 per cent, which exceeds the fidelity of any protocol that does not use entanglement[11]. This demonstration is also important because it incorporates most of the techniques necessary for scalable quantum information processing in an ion-trap system[12,13].

Quantum teleportation[1] provides a means for transporting a quantum state between two separated parties, Alice and Bob, through the transmission of a relatively small amount of classical information. For the case of a two-state quantum system or 'qubit', only two bits of classical information are needed, which seems surprising as precise specification of a general qubit state requires an infinite amount of classical information. Aside from the obvious differences in the various experimental demonstrations, the basic teleportation protocol is the same[1]. Alice is in possession of a qubit (here labelled 2) that is in an unknown state $|\psi\rangle_2 \equiv \alpha|\uparrow\rangle_2 + \beta|\downarrow\rangle_2$, where $|\downarrow\rangle$ and $|\uparrow\rangle$ denote eigenstates of the qubit in the measurement basis. In addition, Alice and Bob each possess one qubit of a two-qubit entangled pair that we take to be a singlet $|S\rangle_{1,3} \equiv |\uparrow\rangle_1|\downarrow\rangle_3 - |\downarrow\rangle_1|\uparrow\rangle_3$ (where, for simplicity, we omit normalization factors). Therefore, Alice possesses qubits 1 and 2, while Bob holds qubit 3. Alice wishes to transmit the state of qubit 2 to Bob's qubit using only classical communication. The initial joint state of all three qubits is

$$|\Phi\rangle = |S\rangle_{1,3} \otimes |\psi\rangle_2. \quad (1)$$

This state can be rewritten using an orthonormal basis of Bell states[14] $|\Psi_k\rangle_{1,2} (k = 1–4)$ for the first two qubits and unitary transformations U_k acting on $|\psi\rangle_3 (= \alpha|\uparrow\rangle_3 + \beta|\downarrow\rangle_3)$ so that $|\Phi\rangle = \Sigma_{k=1}^{4} |\Psi_k\rangle_{1,2} (U_k|\psi\rangle_3)$. A measurement in the Bell-state basis $\{|\Psi_k\rangle\}$ by Alice then leaves Bob with one of the four possibilities $U_k|\psi\rangle_3$. Once Bob learns of Alice's measurement outcome (through classical communication), he can recover the original unknown state by applying the appropriate unitary operator, U_k^{-1}, to his state $U_k|\psi\rangle_3$. We note that Alice's Bell-state measurement can be accomplished by transforming from the basis $\{|\Psi_k\rangle_{1,2}\}$ into the measurement basis $\{|\uparrow\uparrow\rangle_{1,2}, |\uparrow\downarrow\rangle_{1,2}, |\downarrow\uparrow\rangle_{1,2}, |\downarrow\downarrow\rangle_{1,2}\}$ before the measurement.

Our implementation uses atomic qubits ($^9Be^+$ ions) that are confined in a linear radiofrequency Paul trap similar to that used in ref. 15. The control electrodes are segmented into eight sections as shown schematically in Fig. 1, providing a total of six trapping zones (centred on electrode segments 2 to 7). Potentials applied to these electrodes can be varied in time to separate ions and move them to different locations. The qubits are composed of the ground-state hyperfine levels $|\uparrow\rangle \equiv |F = 1, m = -1\rangle$ and $|\downarrow\rangle \equiv |F = 2, m = -2\rangle$, which are separated by $\omega_0 \cong 2\pi \times 1.25\,\mathrm{GHz}$. These states are coupled through stimulated Raman transitions[16–18] from two laser

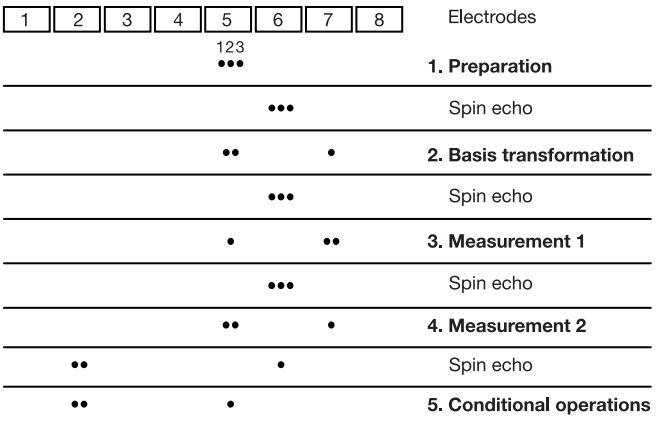

Figure 1 Schematic representation of the teleportation protocol. The ions are numbered left to right, as indicated at the top, and retain their order throughout. Positions, relative to the electrodes, are shown at each step in the protocol. The widths of the electrodes vary, with the width of the separation electrode (6) being the smallest at 100 μm. The spacing between ions in the same trap is about 3 μm, and laser-beam spot sizes (in traps 5 and 6) at the position of the ions are approximately 30 μm. In step 1 we prepare the outer ions in an entangled (singlet) state and the middle ion in an arbitrary state (equation (1)). Steps 2–4 constitute a measurement in a Bell-basis for ions 1 and 2 (Alice's qubits), teleporting the state of ion 2 onto ion 3 (Bob's qubit), up to unitary operations that depend on the measurement outcomes. In step 5 we invoke these conditional operations, recovering the initial state. Interspersed are spin-echo pulses applied in trap 6 that protect the state from de-phasing due to fluctuating magnetic fields but do not affect the teleportation protocol.

beams, which are used to implement the single-qubit rotations

$$R(\theta,\phi) = \cos(\theta/2)I + i\sin(\theta/2)\cos(\phi)\sigma_x + i\sin(\theta/2)\sin(\phi)\sigma_y, \quad (2)$$

where I is the identity operator, σ_x, σ_y and σ_z denote the Pauli spin matrices in the $\{|\uparrow\rangle, |\downarrow\rangle\}$ basis ($\langle\uparrow| \equiv (1,0)$, $\langle\downarrow| \equiv (0,1)$), θ is proportional to the duration of the Raman pulse, and ϕ is the relative phase between the Raman beams at the position of the ion. The Raman beams are also used to generate entanglement between two qubits by implementing the phase gate[18]

$$a|\uparrow\uparrow\rangle + b|\uparrow\downarrow\rangle + c|\downarrow\uparrow\rangle + d|\downarrow\downarrow\rangle \rightarrow a|\uparrow\uparrow\rangle - ib|\uparrow\downarrow\rangle - ic|\downarrow\uparrow\rangle + d|\downarrow\downarrow\rangle. \quad (3)$$

Our teleportation scheme is shown schematically in Fig. 1. We highlight the key elements of the protocol in bold lettering and also include the auxiliary 'spin-echo' pulses[15,18] ($R(\pi,\phi_{SE})$) applied to ions in trap 6. These pulses are required in the experiment to prevent dephasing caused by variations in the ambient magnetic field on a timescale longer than the duration between the spin-echo pulses and, with an appropriate choice of ϕ_{SE}, can compensate phase accumulation due to the presence of a static magnetic-field gradient. As they do not fundamentally affect the teleportation, we omit their effects in the following discussion.

We first prepare the state $|S\rangle_{1,3}\otimes|\downarrow\rangle_2$ in two steps: starting from the state $|\downarrow\downarrow\downarrow\rangle_{1,2,3}$ we combine the gate in equation (3) applied to ions 1 and 3 with rotations to generate[18] the state $(|\downarrow\downarrow\rangle_{1,3} - i|\uparrow\uparrow\rangle_{1,3})\otimes|\downarrow\rangle_2$, followed by implementing individual ion rotations as discussed in ref. 19 to produce $|S\rangle_{1,3}$ from $|\downarrow\downarrow\rangle_{1,3} - i|\uparrow\uparrow\rangle_{1,3}$ (see methods section). For state $|S\rangle_{1,3}\otimes|\downarrow\rangle_2$, ions 1 and 3 are in the singlet, which is invariant under a global rotation. Therefore, a global rotation $R(\theta,\phi)_{1,2,3}$ to all three ions rotates the middle ion without affecting the singlet state of ions 1 and 3, and allows us to produce the state of equation (1) for any α and β with appropriate choices of θ and ϕ.

To teleport the state of ion 2 to ion 3, we start by implementing a Bell-state measurement on Alice's qubits, ions 1 and 2. All three ions are transferred to trap 6 and then separated, with ions 1 and 2 going to trap 5 and ion 3 to trap 7. A phase gate (equation (3)) followed by a $\pi/2$-pulse, $R(\pi/2,0)$, is then applied to ions 1 and 2 in trap 5.

Our previous experiments[15] showed a significant amount of motional-mode heating during the separation process, and the separation was achieved with only a 95% success rate. Aided by a smaller separation electrode in the current trap, we can separate the ions in the desired manner with no detectable failure rate. More importantly, the heating has been significantly reduced and we find that after the separation, the stretch mode of the two ions in trap 5 is in the ground state and the centre-of-mass mode has a mean quantum number of about 1. This enables us to implement the phase gate (equation (3)) between ions 1 and 2 with fidelity greater than 90% and without the need for sympathetic recooling[12,13,17]. Ideally (and in the absence of the spin-echo pulses) this leaves the ions in the state

$$|\uparrow\uparrow\rangle_{1,2}\otimes R(\pi/2,-\pi/2)\sigma_x|\psi\rangle_3 + |\uparrow\downarrow\rangle_{1,2}\otimes R(\pi/2,-\pi/2)\sigma_y|\psi\rangle_3 + i|\downarrow\uparrow\rangle_{1,2}\otimes R(\pi/2,-\pi/2)I|\psi\rangle_3 - |\downarrow\downarrow\rangle_{1,2}\otimes R(\pi/2,-\pi/2)\sigma_z|\psi\rangle_3, \quad (4)$$

where $|\psi\rangle_3 = \alpha|\uparrow\rangle_3 + \beta|\downarrow\rangle_3$.

To complete the Bell-state measurement, we need to detect the states of ions 1 and 2 individually. We recombine all three ions in trap 6 and separate them, with ion 1 being transferred to trap 5 and ions 2 and 3 transferred to trap 7. Detection on ion 1 is then achieved through state-dependent resonance fluorescence measurements[19] ($|\downarrow\rangle$ strongly fluoresces whereas $|\uparrow\rangle$ does not), after which we optically pump the ion back to the state $|\downarrow\rangle_1$. All three ions are then recombined in trap 6 and separated again. For this separation, ions 1 and 2 are transferred to trap 5 and ion 3 is returned to trap 7. As the most recent spin-echo pulse applied in trap 6 transferred the state of ion 1 to $|\uparrow\rangle_1$, a subsequent simultaneous detection of ions 1 and 2 effectively measures the state of ion 2 with error less than 1% due to the presence of ion 1.

To complete the teleportation, we apply unitary operations to ion 3 that depend on the measurement outcomes for ions 1 and 2. We first move ions 1 and 2 to trap 2 and ion 3 to trap 5, where unitary operations consisting of a $\pi/2$-pulse, $R(\pi/2,\pi/2)$, followed by the operators σ_x, σ_y, I, σ_z for the measurement outcomes $|\uparrow\uparrow\rangle_{1,2}$, $|\uparrow\downarrow\rangle_{1,2}$, $|\downarrow\uparrow\rangle_{1,2}$, $|\downarrow\downarrow\rangle_{1,2}$ respectively, are applied. As noted above, the inclusion of the spin-echo pulses does not fundamentally change the teleportation protocol; however for $\phi_{SE} = \pi/2$, we must reorder the operations following the $\pi/2$-pulse, $R(\pi/2,\pi/2)$, to I, σ_z, σ_x, σ_y respectively. A complete experiment is about 4 ms in duration, predominantly due to three elements: the cooling of all three axial modes to the ground state (1 ms), implementing the ion separations and movements (2 ms), and the three detection durations (0.6 ms). In the future, use of smaller trap electrodes to speed up ion-separation and gate operations, coupled with better detection, should considerably increase the speed of the teleportation process.

To demonstrate the full protocol we first teleport the basis states $|\uparrow\rangle_2$ and $|\downarrow\rangle_2$, and achieve a fidelity of about 80% (78 ± 3% for $|\uparrow\rangle$ and 84 ± 2% for $|\downarrow\rangle$ for the data taken in the same run as that shown in Fig. 2). We also perform Ramsey experiments where the first $\pi/2$ pulse (having a variable phase ϕ) is applied to ion 2 (starting in the $|\downarrow\rangle_2$ state) and the second pulse (with a fixed phase) is applied to ion 3 after the teleportation is implemented. That is, $R(\pi/2,\phi)$ is applied to ion 2 and $R(\pi/2,\phi_{fixed})$ is applied to ion 3 after teleportation is completed. Ramsey fringes obtained in this way are shown in Fig. 2. We perform these experiments for $\phi_{fixed} = 0$ and $\pi/2$. From this data, we can extract the teleportation fidelities of the states $|\pm X\rangle$, $|\pm Y\rangle$, which are eigenstates of the operators σ_x and σ_y respectively. From these fidelities and those for the states $|\uparrow\rangle$ and $|\downarrow\rangle$, we determine an average fidelity $\langle F\rangle = 78 \pm 2\%$ for the teleportation process. Furthermore, if we perform the teleportation without the conditional operations, the Ramsey fringes disappear and the teleportation fidelity drops to 1/2, equivalent to Bob making a random guess for the teleported state. There are three dominant mechanisms limiting the final fidelity; imperfect preparation of the initial state $|S\rangle_{1,3}\otimes|\downarrow\rangle_2$, imperfections in the second phase gate due to heating accrued in the separation process, and dephasing of the teleported state due to fluctuating magnetic fields. We have investigated these issues in independent experiments and find that each results in a loss of 8 ± 2% in the fidelity of the final state, consistent

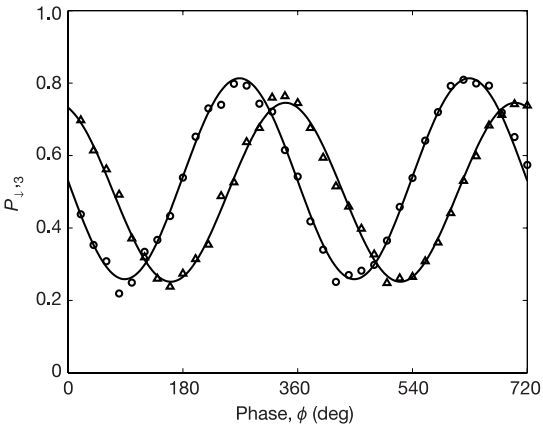

Figure 2 Ramsey fringes demonstrating the teleportation protocol. The two curves correspond to the second Ramsey pulse having $\phi_{fixed} = 0$ (circles) and $\phi_{fixed} = \pi/2$ (triangles) as discussed in the text. We plot the probability $P_{\downarrow,3}$ of observing ion 3 in the $|\downarrow\rangle_3$ state versus the phase of the first Ramsey pulse. Solid curves are best-fit sinusoidal functions to the data. The oscillations of the Ramsey fringes have an amplitude $|\rho_{\downarrow\uparrow}|$ where $\rho_{\downarrow\uparrow} = (\rho_{\uparrow\downarrow})^*$ is the off-diagonal element of the density matrix of the teleported state. The fidelity of the teleported state is then given by $F = 1/2 + |\rho_{\downarrow\uparrow}|$.

with the quoted result for teleportation. In the methods section, we discuss the effects of imperfections in the state preparation and teleportation process.

The average fidelity of 78 ± 2% achieved by our implemented quantum teleportation using atomic qubits, exceeds the value 2/3 necessary to establish the presence of entanglement[11], and is accomplished on demand and without post-selection of the data. Although teleportation has been demonstrated in other systems, our demonstration incorporates the protocol into a simple experiment in such a way that it can be viewed as a subroutine of a quantum algorithm, here, a Ramsey experiment using two separated qubits. Furthermore, our demonstration incorporates most of the important features required for large-scale quantum information processing using trapped ions[12,13]: We (a) reliably select qubits from a group and move them to separate trap zones while maintaining their entanglement, (b) manipulate and detect qubits without the need for strongly focused laser beams, and (c) perform quantum logic operations conditioned on ancilla measurement outcomes. Finally, we note that the University of Innsbruck has also implemented teleportation with the use of three Ca^+ ions in a linear Paul trap[20]. □

Methods

State preparation

Following the protocol outlined in ref. 18, three ions held in trap 5 are first laser-cooled, leaving all three axial modes in the ground state with 99% efficiency[21]. The internal states are then initialized to $|\downarrow\downarrow\downarrow\rangle$ by optical pumping. A motional phase-space 'displacement' pulse, inserted in a spin-echo sequence, is applied to the stretch mode of ions 1 and 3 by Raman beams that have a relative detuning of $\Delta\omega = \omega_s + \delta$, where ω_s is the frequency of the stretch mode and δ is a small detuning as described in ref. 18. The displacement pulse implements the transformation in equation (3) to ions 1 and 3. The spin-echo sequence acts on all three ions: a $\pi/2$-pulse, a delay T_s in which the displacement pulse acts, a π-pulse, an equal time delay T_s, and a final $\pi/2$-pulse. As the amplitude of motion for the middle ion is zero for the stretch mode, the entangling displacement pulse as described has no effect on this ion. Thus the spin-echo pulse sequence leaves the middle ion in the state $|\downarrow\rangle$, while the outer ions are affected as described in ref. 18. For an appropriate choice of detuning, δ, and pulse duration, $T = 2\pi/\delta$, we produce the state $(|\downarrow\downarrow\rangle_{1,3} - i|\uparrow\uparrow\rangle_{1,3})\otimes|\downarrow\rangle_2$ (in the experiment, $T = 9.6\,\mu s$).

To create the state $|S\rangle_{1,3}\otimes|\downarrow\rangle_2$, a second spin-echo sequence is applied with the phase of the pulses shifted by $\pi/4$ with respect to the previous sequence. In addition, for the duration of the middle π-pulse, the axial confinement is changed. The resulting change in each ion's position gives rise to a relative phase of $-\pi/4$, 0, and $+\pi/4$ for ions 1, 2 and 3, respectively[19]. For ion 2, the phase of the π-pulse is the same as the first and last $\pi/2$-pulses and the sequence leaves the ion in the state $|\downarrow\rangle_2$. The outer two ions are initially in the state $|\downarrow\downarrow\rangle_{1,3} - i|\uparrow\uparrow\rangle_{1,3}$ and the first $\pi/2$-pulse yields the state $|\downarrow\uparrow\rangle_{1,3} + |\uparrow\downarrow\rangle_{1,3}$. The π-pulse, with the $\pi/2$ phase difference on ions 1 and 3, results in the singlet state $|\uparrow\downarrow\rangle_{1,3} - |\downarrow\uparrow\rangle_{1,3}$. This state, being invariant under a global rotation, remains unchanged by the final $\pi/2$-pulse. The three-ion state is then the desired state $|S\rangle_{1,3}\otimes|\downarrow\rangle_2$. Auxiliary experiments establish a singlet fidelity $F_S = \mathrm{Tr}_2({}_{1,3}\langle S|\rho_{exp}|S\rangle_{1,3}) \approx 0.92(1)$ and a fidelity for the initial state of ion 2 of $\mathrm{Tr}_{1,3}({}_2\langle\downarrow|\rho\mathrm{exp}|\downarrow\rangle_2) \approx 0.95(1)$.

Imperfect state preparation and teleportation operations

As the operations in the experiment are imperfect, we must examine these effects to show that the observed teleportation fidelity that exceeds 2/3 could not be caused by these imperfections. In particular, as the initial state of ions 1 and 3 is not a perfect singlet, when we rotate all three qubits to prepare the state $|\psi\rangle_2 = \alpha|\uparrow\rangle_2 + \beta|\downarrow\rangle_2$, we could potentially encode this information onto bit 3 even before the teleportation process is started. We address this issue as follows: We can verify that the gate in the state preparation does not entangle bit 2 with bits 1 and 3. Therefore the most general input state is given by

$$|\Psi\rangle_{\mathrm{initial}} = (a_0|\downarrow\downarrow\rangle_{1,3} + a_1|\downarrow\uparrow\rangle_{1,3} + a_2|\uparrow\downarrow\rangle_{1,3} + a_3|\uparrow\uparrow\rangle_{1,3})\otimes(b_0|\downarrow\rangle_2 + b_1|\uparrow\rangle_2), \quad (5)$$

where, ideally, $a_1 = -a_2 = 2^{-1/2}$ and $b_0 = 1$. Here we assume that the subsequent rotation to prepare $|\psi\rangle_2$ and the teleportation operations are perfect. However, in the experiment, after preparation of $|\Psi\rangle_{\mathrm{initial}}$, we switch Raman beams from a geometry where the beams propagate at 90° to each other to a geometry where the beams co-propagate. Owing to fluctuating differences in the optical path lengths between these two sets of beams, there is a random phase difference from experiment to experiment between the corresponding Raman pulses. Over many experiments, some of the coherence terms between all three qubits average out due to this phase randomization, leading to a simplification of the calculated average fidelity with respect to the imperfections in state preparation.

The average fidelity $\langle F\rangle$ is evaluated from the expression

$$\langle F\rangle = (F(|\uparrow\rangle) + F(|\downarrow\rangle) + F(|+X\rangle) + F(|-X\rangle) + F(|+Y\rangle) + F(|-Y\rangle))/6, \quad (6)$$

where the arguments correspond to the initial state, $|\psi\rangle_2$. We find

$$\langle F\rangle = (2 - |b_0|^2)/3 + 2(2|b_0|^2 - 1)F_s/3. \quad (7)$$

When $F_s \leq 1/2$, $\langle F\rangle \leq 2/3$, and we conclude that the teleportation fidelity cannot exceed 2/3 unless the teleportation has occurred through the entangled singlet state as described in the text. Furthermore, imperfect state preparation of ion 2 contributes to an overall loss in fidelity. In a similar way, by simulation, we have also examined the effects of likely imperfections in the teleporting process and conclude that these imperfections only reduce the measured value of $\langle F\rangle$. Therefore, the experimentally measured value of $\langle F\rangle$ indicates that entanglement between bits 1 and 3 was required.

Received 17 March; accepted 4 May 2004; doi:10.1038/nature02608.

1. Bennett, C. H. *et al.* Teleporting an unknown quantum state via dual classical and Einstein-Podolsky-Rosen channels. *Phys. Rev. Lett.* **70,** 1895–1899 (1993).
2. Briegel, H.-J., Dür, W., Cirac, J. I. & Zoller, P. Quantum repeaters: The role of imperfect local operations in quantum communication. *Phys. Rev. Lett.* **81,** 5932–5935 (1998).
3. Gottesman, D. & Chuang, I. L. Demonstrating the viability of universal quantum computation using teleportation and single-qubit operations. *Nature* **402,** 390–393 (1999).
4. Bouwmeester, D. *et al.* Experimental quantum teleportation. *Nature* **390,** 575–579 (1997).
5. Furusawa, A. *et al.* Unconditional quantum teleportation. *Science* **282,** 706–709 (1998).
6. Boschi, D., Branca, S., De Martini, F., Hardy, L. & Popescu, S. Experimental realization of teleporting an unknown pure quantum state via dual classical and Einstein-Podolsky-Rosen channels. *Phys. Rev. Lett.* **80,** 1121–1125 (1998).
7. Kim, Y.-H., Kulik, S. P. & Shih, Y. Quantum teleportation of a polarization state with a complete Bell state measurement. *Phys. Rev. Lett.* **86,** 1370–1373 (2001).
8. Bowen, W. P. *et al.* Experimental investigation of continuous-variable quantum teleportation. *Phys. Rev. A.* **67,** 032302 (2003).
9. Zhang, T. C., Goh, K. W., Chou, C. W., Lodahl, P. & Kimble, H. J. Quantum teleportation of light beams. *Phys. Rev. A* **67,** 033802 (2003).
10. Nielsen, M. A., Knill, E. & Laflamme, R. Complete quantum teleportation using nuclear magnetic resonance. *Nature* **396,** 52–55 (1998).
11. Massar, M. & Popescu, S. Optimal extraction of information from finite quantum ensembles. *Phys. Rev. Lett.* **74,** 1259–1263 (1995).
12. Wineland, D. J. *et al.* Experimental issues in coherent quantum-state manipulation of trapped atomic ions. *J. Res. Natl Inst. Stand. Technol.* **103,** 259–358 (2003).
13. Kielpinski, D., Monroe, C. & Wineland, D. J. Architecture for a large-scale ion-trap quantum computer. *Nature* **417,** 709–711 (2002).
14. Nielsen, M. A. & Chuang, I. L *Quantum Computation and Quantum Information* (Cambridge Univ. Press, Cambridge, 2000).
15. Rowe, M. A. *et al.* Transport of quantum states and separation of ions in a dual rf ion trap. *Quant. Inf. Comp.* **2,** 257–271 (2002).
16. Wineland, D. J. *et al.* Quantum information processing with trapped ions. *Phil. Trans. R. Soc. Lond. A* **361,** 1349–1361 (2003).
17. Barrett, M. D. *et al.* Sympathetic cooling of $^9Be^+$ and $^{24}Mg^+$ for quantum logic. *Phys. Rev. A* **68,** 042302 (2003).
18. Leibfried, D. *et al.* Experimental demonstration of a robust, high-fidelity geometric two ion-qubit phase gate. *Nature* **422,** 412–415 (2003).
19. Rowe, M. A. *et al.* Experimental violation of a Bell's inequality with efficient detection. *Nature* **409,** 791–794 (2001).
20. Riebe, M. *et al.* Deterministic quantum teleportation with atoms. *Nature* (this issue).
21. King, B. E. *et al.* Cooling the collective motion of trapped ions to initialize a quantum register. *Phys. Rev. Lett.* **81,** 1525–1528 (1998).

Acknowledgements This work was supported by ARDA/NSA and NIST. We thank J. Bollinger and J. Martinis for helpful comments on the manuscript. T.S. acknowledges a Deutsche Forschungsgemeinschaft research grant. This paper is a contribution of the National Institute of Standards and Technology and is not subject to US copyright.

Competing interests statement The authors declare that they have no competing financial interests.

Correspondence and requests for materials should be addressed to D.J.W. (djw@boulder.nist.gov)

In situ observation of colloidal monolayer nucleation driven by an alternating electric field

Ke-Qin Zhang & Xiang Y. Liu

Department of Physics, National University of Singapore, 2 Science Drive 3, Singapore 117542

The nucleation of crystalline materials is a hotly debated subject in the physical sciences[1]. Despite the emergence of several theories in recent decades[2–7], much confusion still surrounds the dynamic processes of nucleation[5–7]. This has been due in part to the limitations of existing experimental evidence. Charged

Mars concretion systems. Although the analogue is not a perfect match in every geologic parameter, the mere presence of these spherical haematite concretions implies significant pore volumes of moving subsurface fluids through porous rock.

Haematite is one of the few minerals found on Mars that can be linked directly to water-related processes. Utah haematite concretions are similar to the Mars concretions with spherical morphology, haematite composition, and loose, weathered accumulations. The abundance of quartz in the Utah example could pose challenges for finding spectral matches to the concretions. However, the similarities and differences of the Utah and Mars haematite concretions should stimulate further investigations. The potential role of biomediation in the precipitation of some terrestrial haematite concretions could also hold important clues in the search for life on Mars. Intriguing factors in the Mars system yet to be explored include: spectral comparisons, the source of the iron, the driving mechanism for fluid flow, and other chemical and physical parameters. This Utah analogue presents a model for a fascinating history of fluid flow in the haematite region of Mars. □

Received 18 February; accepted 26 April 2004; doi:10.1038/nature02600.

1. NASA Jet Propulsion Laboratory. *Mars Exploration Rover Mission* ⟨http://marsrovers.jpl.nasa.gov⟩ (February–March 2004).
2. Glotch, T. D. *et al.* Hematite at Meridiani Planum: Detailed spectroscopic observations and testable hypotheses. *Lunar Planet. Sci. Conf. XXXV* [online] Abstr. 2168; ⟨http://www.lpi.usra.edu/meetings/lpsc2004⟩ (2004).
3. Squyres, S. W. *et al.* Initial results from the MER Athena Science investigation at Gusev Crater and Meridiani Planum. *Lunar Planet. Sci. Conf. XXXV* [online] Abstr. 2187, ⟨http://www.lpi.usra.edu/meetings/lpsc2004⟩ (2004).
4. Chan, M. A., Parry, W. T. & Bowman, J. R. Diagenetic hematite and manganese oxides and fault-related fluid flow in Jurassic sandstones, southeastern Utah. *Am. Assoc. Petrol. Geol. Bull.* **84,** 1281–1310 (2000).
5. Chan, M. A. & Parry, W. T. Rainbow of rocks: mysteries of sandstone colors and concretions in Colorado Plateau Canyon Country. (Utah Geological Survey Public Information Service, Salt Lake City, Utah, 2002); ⟨http://www.ugs.state.ut.us/online/pdf/pi-77.pdf⟩.
6. Christensen, P. R., Morris, R. V., Lane, M. D., Bandfield, J. L. & Malin, M. C. Global mapping of Martian hematite mineral deposits: Remnants of water-driven processes on early Mars. *J. Geophys. Res.* **106,** 23873–23885 (2001).
7. Newsom, H. E. *et al.* Paleolakes and impact basins in southern Arabia Terra, including Meridiani Planum: Implications for the formation of hematite deposits on Mars. *J. Geophys. Res.* **108,** doi:10.1029/2002JE001993 (2003).
8. Catling, D. C. & Moore, J. M. The nature of coarse-grained crystalline hematite and its implications for the early environment of Mars. *Icarus* **165,** 277–300 (2003).
9. Hynek, B. M., Arvidson, R. E. & Phillips, R. J. Geological setting and origin of Terra Meridiani hematite deposit on Mars. *J. Geophys. Res.* **107,** doi:10.1029/2002JE001891 (2002).
10. Ormö, J. & Komatsu, G. Hydrocarbon related bleaching of strata and hematite deposition in red beds at Moab, Utah: A possible analogous process that formed bright layers and hematite deposits on Mars. *Lunar Planet. Sci. Conf. XXXIV* [online] Abstr. 1356, ⟨http://www.lpi.usra.edu/meetings/lpsc2003⟩ (2003).
11. Beitler, B., Ormö, J., Komatsu, G., Chan, M. A. & Parry, W. T. Geomorphic and diagenetic analogs to hematite regions on Mars: Examples from Jurassic Sandstones of Southern Utah, USA. *Lunar Planet. Sci. Conf. XXXV* [online] Abstr. 1289, ⟨http://www.lpi.usra.edu/meetings/lpsc2004⟩ (2004).
12. Antonellini, M. & Aydin, A. Effect of faulting on fluid flow in porous sandstones: geometry and spatial distribution. *Am. Assoc. Petrol. Geol. Bull* **79,** 642–671 (1995).
13. Hood, J. W. & Patterson, D. J. *Bedrock Aquifers in the Northern San Rafael Swell Area, Utah, with Special Emphasis on the Navajo Sandstone.* Technical Publication 78 (Utah Department of National Research, 1984).
14. Chan, M. A., Parry, W. T., Petersen, E. U. & Hall, C. M. ^{40}Ar-^{39}Ar age and chemistry of manganese mineralization in the Moab to Lisbon fault systems, southeastern Utah. *Geology* **29,** 331–334 (2001).
15. Beitler, B., Parry, W. T. & Chan, M. A. Bleaching of Jurassic Navajo Sandstone on Colorado Plateau Laramide Highs: Evidence of exhumed hydrocarbon supergiants? *Geology* **31,** 1041–1044 (2003).
16. Parry, W. T., Chan, M. A. & Beitler, B. Chemical bleaching indicates fluid flow in sandstone deformation bands. *Am. Assoc. Petrol. Geol. Bull.* **88,** 175–191 (2004).
17. Beitler, B., Chan, M. A. & Parry, W. T. Field mapping and multispectral analysis of Jurassic Navajo Sandstone color and iron mineralization, Grand Staircase-Escalante National Monument, Utah. *Geol. Soc. Am. Abstr.* **34,** 277 (2002).
18. Ortoleva, P. T. *Geochemical Self-Organization* (Oxford Univ. Press, 1994).
19. Cornell, R. M. & Schwertmann, U. The iron oxides: Structures, properties, reactions, occurrences and uses. (VCH, New York, 1996).
20. Adamovic, J. in *Ironstones Pseudokarst Reports 2* (eds Adamovic, J. & Cilek, V.) 7–40 (Czech Speleological Society, Zlaty Kun, Prague, 2002).
21. Nuccio, V. F. & Condon, S. M. Burial and thermal history of the Paradox Basin, Utah and Colorado, and petroleum potential of the middle Pennsylvanian Paradox Formation. *US Geol. Surv. Bull.* **76,** O1–O41 (1996).
22. Morgan, P. & Gosnold, W. D. in *Geophysical Framework of the Continental United States* (eds Pakiser, L. C. & Mooney, W. D.) 493–522 (Geological Society of America Memoirs Vol. 172, Boulder, Colorado, 1989).
23. Minitti, M. E., Lane, M. D. & Bishop, J. L. A new hematite formation mechanism for Mars. *Lunar Planet. Sci. Conf. XXXV* [online] Abstr. 1999, ⟨http://www.lpi.usra.edu/meetings/lpsc2004⟩ (2004).
24. Hoffman, N. White Mars: A new model for Mars' surface and atmosphere based on CO_2. *Icarus* **146,** 326–342 (2000).
25. Fernández-Remolar, D. *et al.* The Tinto River, an extreme acidic environment under control of iron, as an analog of the Terra Meridiani hematite site of Mars. *Planet. Space Sci.* **53,** 239–248 (2004).

Acknowledgements We thank the donors of the American Chemical Society Petroleum Research Fund, and the Bureau of Land Management-Grand Staircase Escalante National Monument for partial support of this research (to M.A.C. and W.T.P.). The work by J.O. was supported by the Spanish Ministry for Science and Technology and the Ramon y Cajal Program. The work by G.K. was supported by funding from the Italian Space Agency.

Competing interests statement The authors declare that they have no competing financial interests.

Correspondence and requests for materials should be addressed to M.A.C. (machan@mines.utah.edu).

Deterministic quantum teleportation with atoms

M. Riebe[1], H. Häffner[1], C. F. Roos[1], W. Hänsel[1], J. Benhelm[1], G. P. T. Lancaster[1], T. W. Körber[1], C. Becher[1], F. Schmidt-Kaler[1], D. F. V. James[2] & R. Blatt[1,3]

[1]*Institut für Experimentalphysik, Universität Innsbruck, Technikerstraße 25, A-6020 Innsbruck, Austria*
[2]*Theoretical Division T-4, Los Alamos National Laboratory, Los Alamos NM 87545, USA*
[3]*Institut für Quantenoptik und Quanteninformation, Österreichische Akademie der Wissenschaften, Technikerstraße 25, A-6020 Innsbruck, Austria*

Teleportation of a quantum state encompasses the complete transfer of information from one particle to another. The complete specification of the quantum state of a system generally requires an infinite amount of information, even for simple two-level systems (qubits). Moreover, the principles of quantum mechanics dictate that any measurement on a system immediately alters its state, while yielding at most one bit of information. The transfer of a state from one system to another (by performing measurements on the first and operations on the second) might therefore appear impossible. However, it has been shown[1] that the entangling properties of quantum mechanics, in combination with classical communication, allow quantum-state teleportation to be performed. Teleportation using pairs of entangled photons has been demonstrated[2–6], but such techniques are probabilistic, requiring post-selection of measured photons. Here, we report deterministic quantum-state teleportation between a pair of trapped calcium ions. Following closely the original proposal[1], we create a highly entangled pair of ions and perform a complete Bell-state measurement involving one ion from this pair and a third source ion. State reconstruction conditioned on this measurement is then performed on the other half of the entangled pair. The measured fidelity is 75%, demonstrating unequivocally the quantum nature of the process.

Teleportation of a state from a source qubit to a target qubit requires three qubits: the sender's source qubit and an ancillary qubit that is maximally entangled with the receiver's target qubit, providing the strong quantum correlation. Once these states have been prepared, a quantum mechanical measurement is performed jointly on the source qubit and the ancilla qubit (specifically, a Bell-state measurement, which projects the two qubits onto a basis of maximally entangled states). In this process, the two qubits are projected onto one of four equally likely outcomes. At the same time, the non-local properties of quantum mechanics cause the target qubit to be projected onto one of four corresponding states,

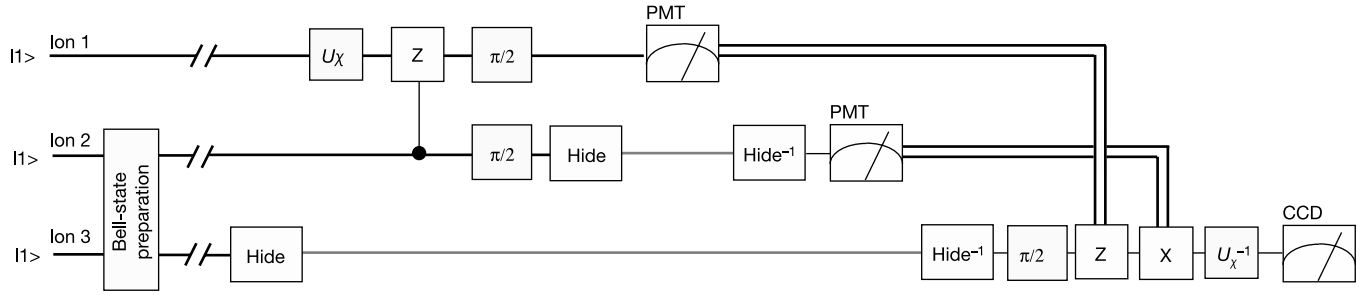

Figure 1 Teleportation from ion 1 to ion 3. A Bell state of ions 2 and 3 is prepared as a resource. The state to be teleported is encoded in ion 1 by the operation U_χ. The Bell-state analyser consists of a controlled Z-gate followed by $\pi/2$ rotations and a state detection of ions 1 and 2. Note that this implementation uses a Bell basis rotated by $\pi/4$ with respect to the standard notation. Therefore a $\pi/2$ rotation on ion 3 is required before the reconstruction operations Z and X. The latter operations are realized by a π rotation around the *z* and *x* axes, respectively. Grey lines indicate qubits that are protected against light scattering. Ions 1 and 2 are detected by observing their fluorescence on a photomultiplier tube (PMT). Only on a detection event $|0\rangle$ is the corresponding reconstruction operation applied to ion 3. Classical information is represented by double lines. For the fidelity analysis we apply U_χ^{-1}, and measure the quantum state of ion 3 by observing its resonance fluorescence using a CCD camera.

each related to the original state of the source qubit, even though no measurement was performed on this qubit. Knowledge of the result of the source-ancilla measurement allows one to choose a simple *a priori* operation to be carried out on the target qubit, resulting in reconstruction of the original quantum state. Because each of the four results on the source-ancilla measurement are equally likely, regardless of the nature of the teleported state, no information about the state is obtained (thus the no-cloning theorem[7] is not violated); further, as classical communication of the measurement outcome is required to complete the state reconstruction, a state cannot be teleported faster than the speed of light. Teleportation does demonstrate a number of fascinating fundamental properties of quantum theory, in particular the non-local property of entangled states, which allows the projective measurement of the source-ancilla pair to create a definite pure state in the target qubit. Furthermore, teleportation has considerable implications for the nascent technology of quantum information processing[8]; besides being a compelling benchmark algorithm for a three-qubit quantum computer, teleportation is a possible primitive for large-scale devices[9].

Experiments demonstrating qubit teleportation[2–6], all of which used photons, were lacking the ability to perform a complete two-photon Bell-state measurement. Successful teleportation events were established by selecting the data after completion of the experiment, searching for the subset of experiments in which the outcome of the measurement and a preset reconstruction operation were matched: that is, teleportation was performed post-selectively. One experiment[10] demonstrated unconditional teleportation of continuous variables, in this case the quadrature amplitudes of a light field. Mention should be made of a liquid-state NMR experiment[11] in which an ensemble of molecules was used in a highly mixed state.

Our implementation of quantum teleportation uses entangled states of massive particles (see also ref. 12). For this, we store three $^{40}Ca^+$ ions in a linear Paul trap; for a detailed description of the experimental set-up, see ref. 13. The ions are arrayed in a linear crystal with an inter-ion distance of 5 μm. A qubit is encoded in a superposition of the $S_{1/2}$ ground state and the metastable $D_{5/2}$ state (lifetime $\tau \approx 1.16$ s) of a $^{40}Ca^+$ ion. Each qubit can be individually manipulated by a series of laser pulses on the $|1\rangle \equiv S_{1/2}(m_J = -1/2)$ to $|0\rangle \equiv D_{5/2}(m_J = -1/2)$ quadrupole transition near 729 nm employing narrow-band laser radiation tightly focused onto individual ions in the string. The qubits are initialized in $|1\rangle$ by optical pumping. The centre-of-mass vibrational mode ($\omega = 2\pi \times 1.2$ MHz) of the ion string is cooled to the ground state as required for controlled interaction between the ions[13].

We teleport the quantum state of ion 1 (the source qubit) onto ion 3 (the target qubit) using the quantum circuit shown in Fig. 1. The sequence is formally equivalent to the one proposed by Bennett *et al.*[1], but adapted to the ion-based quantum processor. As a first step we prepare ion 2 (the ancilla) and 3 in the Bell state $|\psi_+\rangle_{23} = (|0\rangle_2|1\rangle_3 + |1\rangle_2|0\rangle_3)/\sqrt{2}$, the lifetime of which exceeds 100 ms

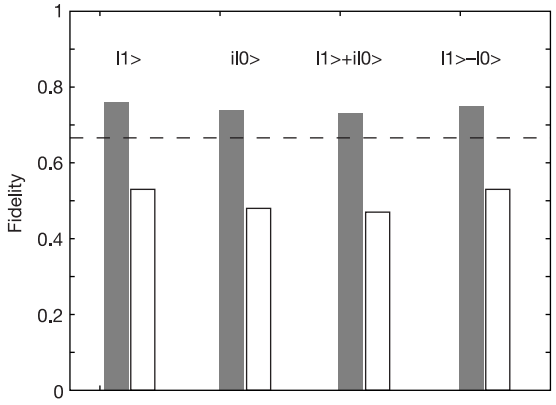

Figure 2 Result of the teleportation. The four test states are teleported with fidelities of 76%, 74%, 73% and 75%, respectively (grey bars). For each input state, 300 single teleportation experiments were performed. The error of each entry, estimated from quantum projection noise, is 2.5%. For comparison, white bars show the results if the reconstruction operations are omitted, yielding an average fidelity of 49.6%. The optimum 'teleportation' obtainable by purely classical means reaches a fidelity of 66.7% (dashed line).

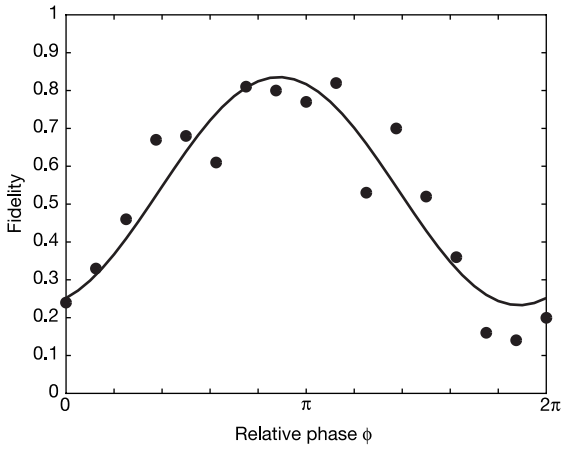

Figure 3 Fidelity of teleportation as a function of the relative phase ϕ of the reconstruction and analysing pulses (see Table 1). This is demonstrated for the test input state $|1\rangle$. Varying ϕ is used for optimizing the experimental fidelity thus accounting for a residual uncompensated phase drift during the entire process (which is the same for all input states).

(ref. 14). Then, at any time within this lifetime, the actual teleportation step—taking less than 2 ms—can be carried out: Ion 1 is prepared in an arbitrary input state with local rotations. In our experiments the teleported state $|\chi\rangle$ was one of a set of four non-orthogonal test states $|\chi^{(1)}\rangle = |1\rangle$, $|\chi^{(2)}\rangle = |0\rangle$, $|\chi^{(3)}\rangle = (|0\rangle + |1\rangle)/\sqrt{2}$ and $|\chi^{(4)}\rangle = (i|0\rangle + |1\rangle)/\sqrt{2}$. The Bell-state analysis is implemented by a controlled phase gate between ion 1 and 2 (ref. 11) followed by a $\pi/2$ pulse on each ion. Then the joint quantum state of ions 1 and 2 is measured by illuminating them with light at 397 nm for 250 μs. Detection of fluorescence indicates the projection of the ion's quantum state into the $S_{1/2}$ state, (logical $|1\rangle$), whereas the absence of fluorescence indicates its projection into the $|0\rangle$ state with nearly 100% detection efficiency. Fluorescence is collected with a photomultiplier tube and the result is stored electronically. The measurement process must preserve the coherence of the target qubit, ion 3. Thus, the state of ion 3 is hidden by transferring it to a superposition of levels that are not affected by the detection light. In Ca^+, an additional Zeeman level $|H\rangle \equiv D_{5/2}(m_J = -5/2)$ can be used for this purpose by moving any $S_{1/2}$ population into the $|H\rangle$ level. The same technique is used to sequentially read out ion 1 and ion 2 and discriminate between all four possible states $\{|0\rangle_1|0\rangle_2, |0\rangle_1|1\rangle_2, |1\rangle_1|0\rangle_2, |1\rangle_1|1\rangle_2\}$. Conditional on the measurement outcome, we apply the appropriate unitary qubit rotation, $-i\sigma_y$, $-i\sigma_z$, $i\sigma_x$ or 1 (with Pauli operators σ_k) to reconstruct the state in the target ion 3, obtaining $|\chi^{(\mathrm{exp})}\rangle$. We emphasize that this conditional, deterministic step, in combination with the complete Bell-state analysis, is one of the crucial improvements with respect to all former experimental realizations of quantum teleportation with qubits. Furthermore, after the teleportation procedure the state $|\chi\rangle$ is always available and may be used for further experiments.

Table 1 **Pulse sequence of the teleportation protocol.**

	Action	Comment
1	Light at 397 nm	Doppler preparation
2	Light at 729 nm	Sideband cooling
3	Light at 397 nm	Optical pumping
Entangle		
4	$R_3^+(\pi/2, 3\pi/2)$	Entangle ion 3 with motional qubit
5	$R_2^C(\pi, 3\pi/2)$	Prepare ion 2 for entanglement
6	$R_2^+(\pi, \pi/2)$	Entangle ion 2 with ion 3
7	Wait for 1 μs – 10,000 μs	Standby for teleportation
8	$R_3^H(\pi, 0)$	Hide target ion
9	$R_1^C(\vartheta_\chi, \varphi_\chi)$	Prepare source ion 1 in state χ
Rotate into Bell basis		
10	$R_2^+(\pi, 3\pi/2)$	Get motional qubit from ion 2
11	$R_1^+(\pi/\sqrt{2}, \pi/2)$	Composite pulse for phasegate
12	$R_1^+(\pi, 0)$	Composite pulse for phasegate
13	$R_1^+(\pi/\sqrt{2}, \pi/2)$	Composite pulse for phasegate
14	$R_1^+(\pi, 0)$	Composite pulse for phasegate
15	$R_1^C(\pi, \pi/2)$	Spin echo on ion 1
16	$R_3^H(\pi, \pi)$	Unhide ion 3 for spin echo
17	$R_3^C(\pi, \pi/2)$	Spin echo on ion 3
18	$R_3^H(\pi, 0)$	Hide ion 3 again
19	$R_2^+(\pi, \pi/2)$	Write motional qubit back to ion 2
20	$R_1^C(\pi/2, 3\pi/2)$	Part of rotation into Bell basis
21	$R_2^C(\pi/2, \pi/2)$	Finalize rotation into Bell basis
Read out		
22	$R_2^H(\pi, 0)$	Hide ion 2
23	PMDetection for 250 μs	Read out of ion 1 with photomultiplier
24	$R_1^H(\pi, 0)$	Hide ion 1
25	$R_2^H(\pi, \pi)$	Unhide ion 2
26	PMDetection for 250 μs	Read out of ion 2 with photomultiplier
27	$R_2^H(\pi, 0)$	Hide ion 2
28	Wait 300 μs	Let system rephase; part of spin echo
29	$R_3^H(\pi, \pi)$	Unhide ion 3
30	$R_3^C(\pi/2, 3\pi/2 + \phi)$	Change basis
Reconstruction		
31	$R_3^C(\pi, \phi)$	$i\sigma_x$ }
32	$R_3^C(\pi, \pi/2 + \phi)$	$-i\sigma_y$ } = $-i\sigma_z$ conditioned on PM detection 1
33	$R_3^C(\pi, \phi)$	$i\sigma_x$ conditioned on PM detection 2
34	$R_3^C(\vartheta_\chi, \varphi_\chi + \pi + \phi)$	Inverse of preparation of χ with offset ϕ
35	Light at 397 nm	Read out of ion 3 with camera

To obtain directly the fidelity of the teleportation, we perform on ion 3 the inverse of the unitary operation $U_\chi \equiv |\chi\rangle\langle 1| + |\bar{\chi}\rangle\langle 0|, (\langle\chi|\bar{\chi}\rangle = 0)$ used to create the input state from state $|1\rangle$. The teleportation is successful if ion 3 is always found in $|1\rangle$. The teleportation fidelity, given by the overlap $F = \langle 1|U_\chi^{-1}\rho_{\mathrm{exp}}U_\chi|1\rangle$, is plotted in Fig. 2 for all four test states. The obtained fidelities range from 73% to 76%. Teleportation based on a completely classical resource instead of a quantum-entangled resource yields[15] a maximal possible average fidelity of 66.7% (dashed line in Fig. 2). Note, however, to rule out hidden variable theories, a fidelity in excess of 0.87 is required[16]. This level of fidelity could be reached by improving primarily the magnetic-field stability and the laser-frequency noise. For comparison, we also show data where the reconstruction pulses were not applied. Without the classical information communicated from the Bell measurement, the receiver's state is maximally mixed, that is there is no information available on the source state. Also, the measurement outcomes of ions 1 and 2 do not contain any information about the initial state $|\chi\rangle$. Indeed, we find each possible result with equal probability of 0.25 ± 0.036, independent of the test input states. Note that only with both the receiver's qubit and the result of the Bell measurement, can the initial state be retrieved.

After the initial Bell-state preparation, only single qubit operations are performed on the target ion (see Fig. 1). Thus, although the scheme presented here takes place in a confining potential common to all three ions, it would, in principle, be possible to separate the target ion from the other two ions. This could be realized in segmented microtrap designs as developed previously[17], which allow separating single ions from a crystal.

To illustrate further the quantum coherence of the teleportation process, we measure its fidelity as a function of the phase of the reconstructing and analysing pulses (see Fig. 3). The oscillation of the teleportation fidelity proves the phase relationship between source and target qubit and thus the quantum nature of the process.

To emphasize the role of the shared entangled pair as a resource, we store the Bell state for some time and then use it only later (after up to 10 ms) for teleportation. For waiting times up to 10 ms (exceeding the time we require for the teleportation by a factor of 5) we observe no decrease in the fidelity. Thus for future quantum-information processing networks, and with entangled states as a resource, quantum teleportation can be used for the distribution of quantum information between different nodes of the network. □

Methods

Pulse sequence

To implement the teleporation we use pulses on carrier transitions $R_i^C(\vartheta, \varphi)$ and $R_i^H(\vartheta, \varphi)$ (no change of the motional state of the ion crystal) and, additionally, on the blue sideband $R_i^+(\vartheta, \varphi)$ (change of the motional state) on ion i. The index C denotes carrier transitions between the two logical eigenstates, and the index H labels the transition from the $S_{1/2}$ ($m_J = -1/2$) to the $D_{5/2}$ ($m_J = -5/2$) level in the Zeeman manifold. For the definitions of $R_i^{C,H,+}(\vartheta, \varphi)$ see refs 13 and 18. In contrast to Fig. 1, in the pulse sequence (Table 1) also the spin-echo pulses[19] are included. These pulses make the algorithm more robust against detunings caused by slow laser and magnetic-field drifts. The timing of these generalized spin-echo pulses was found by optimizing the robustness of the sequence against detunings numerically and experimentally. The conditioned pulses 31,32,33 are applied only if less than six photon detection events were recorded during the respective detection time. For this purpose an electronic circuit counts the pulses of the photomultiplier tube and modifies the pulse sequence accordingly.

Received 17 March; accepted 16 April 2004; doi:10.1038/nature02570.

1. Bennett, C. H. *et al.* Teleporting an unknown quantum state via dual classical and EPR channels. *Phys. Rev. Lett.* **70,** 1895–1899 (1993).
2. Bouwmeester, D. *et al.* Experimental quantum teleportation. *Nature* **390,** 575–579 (1997).
3. Boschi, D., Branca, S., DeMartini, F., Hardy, L. & Popescu, S. Experimental realization of teleporting an unknown pure quantum state via dual classical and Einstein-Podolsky-Rosen channels. *Phys. Rev. Lett.* **80,** 1121–1125 (1998).
4. Pan, J.-W., Daniell, M., Gasparoni, S., Weihs, G. & Zeilinger, A. Experimental demonstration of four-photon entanglement and high-fidelity teleportation. *Phys. Rev. Lett.* **86,** 4435–4438 (2001).
5. Marcikic, I., de Riedmatten, H., Tittel, W., Zbinden, H. & Gisin, N. Long-distance teleportation of qubits at telecommunication wavelengths. *Nature* **421,** 509–513 (2003).
6. Fattal, D., Diamanti, E., Inoue, K. & Yamamoto, Y. Quantum teleportation with a quantum dot single photon source. *Phys. Rev. Lett.* **92,** 037904 (2004).

7. Wootters, W. K. & Zurek, W. H. A single quantum cannot be cloned. *Nature* **299,** 802–803 (1982).
8. Nielsen, M. A. & Chuang, I. J. *Quantum Computation and Quantum Information* (Cambridge Univ. Press, Cambridge, 2000).
9. Gottesman, D. & Chuang, I. L. Demonstrating the viability of universal quantum computation using teleportation and single-qubit operations. *Nature* **402,** 390–393 (1999).
10. Furusawa, A. *et al.* Unconditional quantum teleportation. *Science* **282,** 706–709 (1998).
11. Nielsen, M. A., Knill, E. & Laflamme, R. Complete quantum teleportation using nuclear magnetic resonance. *Nature* **396,** 52–55 (1998).
12. Barrett, M. D. *et al.* Quantum teleportation with atomic qubits. *Nature* (this issue).
13. Schmidt-Kaler, F. *et al.* How to realize a universal quantum gate with trapped ions. *Appl. Phys. B* **77,** 789–796 (2003).
14. Roos, C. F. *et al.* Bell states of atoms with ultra long lifetimes and their tomographic state analysis. *Phys. Rev. Lett.* (in the press) Preprint at ⟨http://arXiv.org/abs/ physics/0307210⟩ (2003).
15. Massar, S. & Popescu, S. Optimal extraction of information from finite quantum ensembles. *Phys. Rev. Lett.* **74,** 1259–1263 (1995).
16. Gisin, N. Nonlocality criteria for quantum teleportation. *Phys. Lett. A* **210,** 157–159 (1996).
17. Kielpinski, D., Monroe, C. & Wineland, D. J. Architecture for a large-scale ion-trap quantum computer. *Nature* **417,** 709–711 (2002).
18. Gulde, S. *et al.* Implementation of the Deutsch-Jozsa algorithm on an ion-trap quantum computer. *Nature* **412,** 48–50 (2003).
19. Hahn, E. L. Spin Echoes. *Phys. Rev.* **80,** 580–594 (1950).

Acknowledgements We thank H. Briegel and P. Zoller for a critical reading of the manuscript. We gratefully acknowledge support by the Austrian Science Fund (FWF), by the European Commission (QUEST, QUBITS and QGATES networks), by the Institut für Quanteninformation, and by the Los Alamos LDRD Program. This material is based upon work supported in part by the US Army Research Office. H.H is funded by the Marie-Curie program of the European Union.

Competing interests statement The authors declare that they have no competing financial interests.

Correspondence and requests for materials should be addressed to R.B. (Rainer.Blatt@uibk.ac.at)

Deterministic quantum teleportation of atomic qubits

M. D. Barrett[1]*, J. Chiaverini[1], T. Schaetz[1], J. Britton[1], W. M. Itano[1], J. D. Jost[1], E. Knill[2], C. Langer[1], D. Leibfried[1], R. Ozeri[1] & D. J. Wineland[1]

[1]*Time and Frequency Division, NIST, Boulder, Colorado 80305, USA*
[2]*Mathematical and Computational Sciences Division, NIST, Boulder, Colorado 80305, USA*

* Present address: Department of Physics, University of Otago, PO Box 56, Dunedin, New Zealand

Quantum teleportation[1] provides a means to transport quantum information efficiently from one location to another, without the physical transfer of the associated quantum-information carrier. This is achieved by using the non-local correlations of previously distributed, entangled quantum bits (qubits). Teleportation is expected to play an integral role in quantum communication[2] and quantum computation[3]. Previous experimental demonstrations have been implemented with optical systems that used both discrete and continuous variables[4–9], and with liquid-state nuclear magnetic resonance[10]. Here we report unconditional teleportation[5] of massive particle qubits using atomic ($^9Be^+$) ions confined in a segmented ion trap, which aids individual qubit addressing. We achieve an average fidelity of 78 per cent, which exceeds the fidelity of any protocol that does not use entanglement[11]. This demonstration is also important because it incorporates most of the techniques necessary for scalable quantum information processing in an ion-trap system[12,13].

Quantum teleportation[1] provides a means for transporting a quantum state between two separated parties, Alice and Bob, through the transmission of a relatively small amount of classical information. For the case of a two-state quantum system or 'qubit', only two bits of classical information are needed, which seems surprising as precise specification of a general qubit state requires an infinite amount of classical information. Aside from the obvious differences in the various experimental demonstrations, the basic teleportation protocol is the same[1]. Alice is in possession of a qubit (here labelled 2) that is in an unknown state $|\psi\rangle_2 \equiv \alpha|\uparrow\rangle_2 + \beta|\downarrow\rangle_2$, where $|\downarrow\rangle$ and $|\uparrow\rangle$ denote eigenstates of the qubit in the measurement basis. In addition, Alice and Bob each possess one qubit of a two-qubit entangled pair that we take to be a singlet $|S\rangle_{1,3} \equiv |\uparrow\rangle_1|\downarrow\rangle_3 - |\downarrow\rangle_1|\uparrow\rangle_3$ (where, for simplicity, we omit normalization factors). Therefore, Alice possesses qubits 1 and 2, while Bob holds qubit 3. Alice wishes to transmit the state of qubit 2 to Bob's qubit using only classical communication. The initial joint state of all three qubits is

$$|\Phi\rangle = |S\rangle_{1,3} \otimes |\psi\rangle_2. \quad (1)$$

This state can be rewritten using an orthonormal basis of Bell states[14] $|\Psi_k\rangle_{1,2} (k = 1–4)$ for the first two qubits and unitary transformations U_k acting on $|\psi\rangle_3 (= \alpha|\uparrow\rangle_3 + \beta|\downarrow\rangle_3)$ so that $|\Phi\rangle = \Sigma_{k=1}^{4} |\Psi_k\rangle_{1,2} (U_k|\psi\rangle_3)$. A measurement in the Bell-state basis $\{|\Psi_k\rangle\}$ by Alice then leaves Bob with one of the four possibilities $U_k|\psi\rangle_3$. Once Bob learns of Alice's measurement outcome (through classical communication), he can recover the original unknown state by applying the appropriate unitary operator, U_k^{-1}, to his state $U_k|\psi\rangle_3$. We note that Alice's Bell-state measurement can be accomplished by transforming from the basis $\{|\Psi_k\rangle_{1,2}\}$ into the measurement basis $\{|\uparrow\uparrow\rangle_{1,2}, |\uparrow\downarrow\rangle_{1,2}, |\downarrow\uparrow\rangle_{1,2}, |\downarrow\downarrow\rangle_{1,2}\}$ before the measurement.

Our implementation uses atomic qubits ($^9Be^+$ ions) that are confined in a linear radiofrequency Paul trap similar to that used in ref. 15. The control electrodes are segmented into eight sections as shown schematically in Fig. 1, providing a total of six trapping zones (centred on electrode segments 2 to 7). Potentials applied to these electrodes can be varied in time to separate ions and move them to different locations. The qubits are composed of the ground-state hyperfine levels $|\uparrow\rangle \equiv |F = 1, m = -1\rangle$ and $|\downarrow\rangle \equiv |F = 2, m = -2\rangle$, which are separated by $\omega_0 \cong 2\pi \times 1.25\,\mathrm{GHz}$. These states are coupled through stimulated Raman transitions[16–18] from two laser

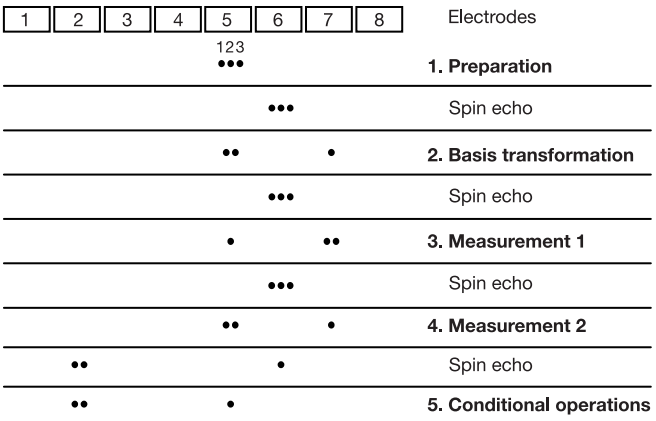

Figure 1 Schematic representation of the teleportation protocol. The ions are numbered left to right, as indicated at the top, and retain their order throughout. Positions, relative to the electrodes, are shown at each step in the protocol. The widths of the electrodes vary, with the width of the separation electrode (6) being the smallest at 100 μm. The spacing between ions in the same trap is about 3 μm, and laser-beam spot sizes (in traps 5 and 6) at the position of the ions are approximately 30 μm. In step 1 we prepare the outer ions in an entangled (singlet) state and the middle ion in an arbitrary state (equation (1)). Steps 2–4 constitute a measurement in a Bell-basis for ions 1 and 2 (Alice's qubits), teleporting the state of ion 2 onto ion 3 (Bob's qubit), up to unitary operations that depend on the measurement outcomes. In step 5 we invoke these conditional operations, recovering the initial state. Interspersed are spin-echo pulses applied in trap 6 that protect the state from de-phasing due to fluctuating magnetic fields but do not affect the teleportation protocol.

LETTERS

Quantum teleportation between light and matter

Jacob F. Sherson[1,3], Hanna Krauter[1], Rasmus K. Olsson[1], Brian Julsgaard[1], Klemens Hammerer[2], Ignacio Cirac[2] & Eugene S. Polzik[1]

Quantum teleportation[1] is an important ingredient in distributed quantum networks[2], and can also serve as an elementary operation in quantum computers[3]. Teleportation was first demonstrated as a transfer of a quantum state of light onto another light beam[4–6]; later developments used optical relays[7] and demonstrated entanglement swapping for continuous variables[8]. The teleportation of a quantum state between two single material particles (trapped ions) has now also been achieved[9,10]. Here we demonstrate teleportation between objects of a different nature—light and matter, which respectively represent 'flying' and 'stationary' media. A quantum state encoded in a light pulse is teleported onto a macroscopic object (an atomic ensemble containing 10^{12} caesium atoms). Deterministic teleportation is achieved for sets of coherent states with mean photon number (n) up to a few hundred. The fidelities are 0.58 ± 0.02 for $n = 20$ and 0.60 ± 0.02 for $n = 5$—higher than any classical state transfer can possibly achieve[11]. Besides being of fundamental interest, teleportation using a macroscopic atomic ensemble is relevant for the practical implementation of a quantum repeater[2]. An important factor for the implementation of quantum networks is the teleportation distance between transmitter and receiver; this is 0.5 metres in the present experiment. As our experiment uses propagating light to achieve the entanglement of light and atoms required for teleportation, the present approach should be scalable to longer distances.

Quantum teleportation—a disembodied transfer of a quantum state with the help of distributed entanglement—was proposed in a seminal paper[1]. The generic protocol of quantum teleportation begins with the creation of a pair of entangled objects which are shared by two parties, Alice and Bob. This step establishes a quantum link between them. Alice receives an object to be teleported and performs a joint measurement on this object and her entangled object (a Bell measurement). The result of this measurement is communicated via a classical communication channel to Bob, who uses it to perform local operations on his entangled object, thus completing the process of teleportation.

In our experiment, a pair of entangled objects is created by sending a strong 'in' pulse of light (shown on the left in Fig. 1) through an atomic sample at Bob's location. As a result of the interaction between the light and the atoms, the transmitted 'out' light received by Alice's and Bob's atoms become entangled. On Alice's site the entangled pulse is mixed with the pulse to be teleported on a 50/50 beamsplitter (BS in Fig. 1). A Bell measurement in the form of homodyne measurements of the optical fields in the two output ports of the BS is carried out and the results are transferred to Bob as classical photocurrents. Bob performs spin rotations on the atoms to complete the teleportation protocol. Finally, the state of the atoms is analysed to confirm that the teleportation has been successful.

The experiment follows a recent proposal for light-to-atoms teleportation[12] using multimode entanglement of light with an atomic ensemble placed in a magnetic field. We describe teleportation in the language of dimensionless canonical variables[13]; this provides a common description for light and atoms, and allows for a complete tomographic characterization of the states.

The atomic object is a spin-polarized gas sample of approximately $N_{at} = 10^{12}$ caesium atoms in a $25 \times 25 \times 25$ mm paraffin-coated glass cell at around room temperature[14–18] placed in a homogeneous magnetic field (**B**). Atoms are initially prepared in a coherent spin state by a 4-ms circularly polarized optical pumping pulse propagating along the direction of the magnetic field, into the sublevel $F = 4, m_F = 4$ (Fig. 1) of the ground state with the collective ensemble angular momentum $\langle \hat{J}_x \rangle = J_x = 4N_{at}$, and the transverse projections with minimal quantum uncertainties, $\langle \delta J_y^2 \rangle = \langle \delta J_z^2 \rangle = \frac{1}{2} J_x$. Changing to the frame rotating at the Larmor frequency Ω and introducing the canonical variables for the collective transverse atomic spin components[12], we obtain $\hat{X}_A = \hat{J}_y^{rot}/\sqrt{J_x}, \hat{P}_A = \hat{J}_z^{rot}/\sqrt{J_x}$ which obey

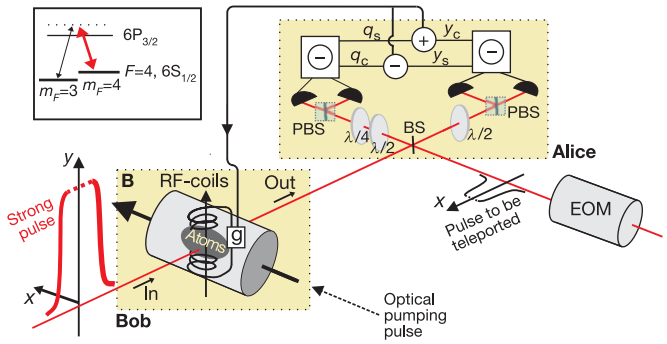

Figure 1 | Experimental set-up for teleportation of light onto an atomic ensemble. Atoms are initially optically pumped into $F = 4$, $m_F = 4$ state with a 4-ms pulse. A strong y-polarized 2-ms 'in' pulse of light is then sent through the atomic sample at Bob's location and becomes entangled with the atoms (the pulse length is around 600 km and is not shown to scale in the figure). The pulse travels 0.5 m to Alice's location, where it is mixed on a beamsplitter (BS) with the object of teleportation—a few-photon coherent pulse of light—generated by the electro-optical modulator (EOM) synchronously with the strong pulse. In the two output ports of the BS, two polarization beamsplitters (PBS) split light onto two pairs of detectors which perform a polarization homodyne measurement (a Bell measurement). The results of these measurements are combined, processed electronically, as described in the text, and sent via a classical communication channel to Bob. There they are used to complete the teleportation onto atoms by shifting the atomic collective spin state with a pulse of a radio-frequency (RF) magnetic field of 0.2-ms duration. After a delay of 0.1 ms, a second strong pulse—the verifying pulse—is sent to read out the atomic state, in order to prove the successful teleportation. Inset, relevant atomic sublevels and light modes (not to scale). The frequency difference between a weak quantum field (black arrow) and the strong entangling field (thick red arrow) is equal to the Zeeman splitting of the ground state sublevels.

[1]Niels Bohr Institute, Copenhagen University, Blegdamsvej 17, Copenhagen Ø, Denmark. [2]Max Planck Institute for Quantum Optics, Hans-Kopfermann-Str. 1, Garching, D-85748, Germany. [3]Department of Physics and Astronomy, University of Aarhus, Aarhus, 8000, Denmark.

the canonical commutation relation $[\hat{X}_A, \hat{P}_A] = i$ provided that $J_x >> \sqrt{\langle \delta J_{y,z}^2 \rangle}, \langle J_{y,z} \rangle$. Here $\hat{X}_A$ and $\hat{P}_A$ are the recipient operators in the teleportation protocol.

The light to be teleported, and the 'in' and 'out' modes (Fig. 1), are described by single mode canonical operators[6,12] $\hat{Y}, \hat{Q}$, and $\hat{y}^{in}, \hat{q}^{in}$ and $\hat{y}^{out}, \hat{q}^{out}$, respectively. These operators obeying $[\hat{Y}, \hat{Q}] = [\hat{y}, \hat{q}] = i$ are quantum analogues of the amplitude and phase of light in classical physics, or, more precisely, of the classical quadrature phase amplitudes y, q in the decomposition of the electric field of light with the frequency ω as $E \propto y \cos \omega t + q \sin \omega t$ (see Methods for exact definitions). Two non-commuting variables in quantum mechanics cannot be measured without distortion. The challenge of teleportation thus consists of a faithful transfer of these not simultaneously measurable operators, $\hat{Y}, \hat{Q}$, onto atomic operators $\hat{X}_A$ and $\hat{P}_A$. The Raman-type interaction (see Fig. 1 inset) couples the quantum $\omega + \Omega$ sideband of the 'in' field to the Zeeman sublevels separated by the frequency $\Omega = 322$ kHz. Therefore we introduce the $\cos \Omega t$, $\sin \Omega t$ components of the light operators $\hat{Y}_{c,s}, \hat{Q}_{c,s}$ and $\hat{y}_{c,s}, \hat{q}_{c,s}$ (see Methods). Canonical operators for the upper sideband mode $\hat{Y}, \hat{Q}$ can be expressed[12] via measurable $\sin(\Omega t)$ and $\cos(\Omega t)$ components, $\hat{Y}_s, \hat{Q}_s, \hat{Y}_c, \hat{Q}_c$, as $\hat{Y} = \frac{1}{\sqrt{2}}(\hat{Y}_s + \hat{Q}_c), \hat{Q} = -\frac{1}{\sqrt{2}}(\hat{Y}_c - \hat{Q}_s)$.

We first describe generation of entanglement between light and atoms. The 'in' strong pulse is y-polarized, hence its x-polarized mode $\hat{y}^{in}, \hat{q}^{in}$ is in a vacuum state. After interaction with atoms[12], the x-polarized 'out' mode operators $\hat{y}^{out}, \hat{q}^{out}$ are given by:

$$\hat{y}_c^{out} = \left\{ \hat{y}_c^{in} + \frac{\kappa^2}{4}\hat{q}_s^{in} + \frac{\kappa^2}{4\sqrt{3}}\nu_s \right\} + \frac{\kappa}{\sqrt{2}}\hat{P}_A^{in}, \qquad \hat{q}_{s,c}^{out} = \hat{q}_{s,c}^{in}$$
$$\hat{y}_s^{out} = \left\{ \hat{y}_s^{in} - \frac{\kappa^2}{4}\hat{q}_c^{in} - \frac{\kappa^2}{4\sqrt{3}}\nu_c \right\} - \frac{\kappa}{\sqrt{2}}\hat{X}_A^{in} \quad (1)$$

The terms in curly brackets in the equations for $\hat{y}$ represent vacuum contributions coming from different orthogonal modes of the 'in' pulse where the canonical operators $\nu_{s,c}$ represent vacuum temporal higher order canonical modes[12]. The terms containing $\hat{P}_A^{in}$ and $\hat{X}_A^{in}$ describe the imprint of the atomic state on the light via coherent forward scattering from the atomic ensemble, or, in other words, polarization rotation due to the Faraday effect[14,15]. The atomic spin operators are transformed by the interaction with light as follows[12]:

$$\hat{X}_A^{out} = \hat{X}_A^{in} + \frac{\kappa}{\sqrt{2}}\hat{q}_c^{in}, \quad \hat{P}_A^{out} = \hat{P}_A^{in} + \frac{\kappa}{\sqrt{2}}\hat{q}_s^{in} \quad (2)$$

The second terms in equation (2) describe the imprint of the light state onto atoms via the dynamic Stark effect[14].

The atoms–light entanglement described by equations (1) and (2) is very close[12], under our experimental conditions, to the Einstein–Podolsky–Rosen entanglement optimal for quantum teleportation. The atoms–light coupling constant $\kappa = a_1\sqrt{N_{ph}N_{at}F\sigma\Gamma/A\Delta} \propto \alpha_0$ has been discussed in detail previously[12,14–18]. (Here σ is the dipole cross-section[18], a_1 is the vector polarizability[18], $\Gamma = 2.6$ MHz is the natural linewidth (HWHM) of the transition, $N_{ph} = 4 \times 10^{13}$ is the number of the y-polarized photons in the strong pulse, $\Delta = 825$ MHz is the blue detuning of light from the atomic resonance, and $A = 4.8\,\mathrm{cm}^2$ is the cross-section of the atomic sample.) As in our previous experiments with the atoms–light quantum interface, strong coupling with the atomic ensemble is achieved in the region of a high resonant optical depth α_0. In the experiment we choose a nearly optimal value[12] of $\kappa \approx 1$ by changing $\alpha_0 \propto N_{at}$ with the temperature of the vapour. Note that another condition for strong coherent coupling is a very high N_{ph} in the y-polarized mode.

At Alice's location (Fig. 1), the 'out' pulse is mixed on BS with the object of teleportation—a few-photon x-polarized coherent pulse with frequency $\omega + \Omega$ generated by an electro-optical modulator (EOM). A Bell measurement of canonical variables[6,12,13] is performed by two sets of polarization homodyne detectors in the two output ports of BS (Fig. 1). Homodyne detection followed by the normalization to the vacuum (shot) noise of light[6] is a standard method for measuring canonical variables of light. In our experiment, the strong y-polarized pulse, besides driving the entangling interaction, also plays the role of a local oscillator for the homodyne detection. The variables in phase with the strong pulse $\hat{y}_{c,s} = \frac{1}{\sqrt{2}}(\hat{y}_{c,s}^{out} + \hat{Y}_{c,s})$ are measured via a measurement of the Stokes parameter $\hat{S}_2$ in one output of BS, whereas the out-of-phase components $\hat{q}_{c,s} = \frac{1}{\sqrt{2}}(\hat{q}_{c,s}^{out} - \hat{Q}_{c,s})$ are measured via the Stokes parameter $\hat{S}_3$ in the other arm (see Methods). The $\sin(\Omega t)$ and $\cos(\Omega t)$ components are measured by processing photocurrents with lock-in amplifiers. The Bell measurement of operators $\hat{y}_{c,s}$ and $\hat{q}_{c,s}$ yields four results, $y_{c,s}$ and $q_{c,s}$. Operationally, these values are properly normalized integrals of corresponding photocurrents over the pulse duration (see Methods). As shown in Fig. 1, the photocurrents are combined to yield two feedback signals proportional to $y_s - q_c$ and $y_c + q_s$ which are sent from Alice to Bob. Auxiliary magnetic field pulses[14,17] with frequency Ω and amplitudes proportional to the feedback signals are applied to the atoms, so that the collective atomic spin variables at Bob's site are shifted to become:

$$\hat{X}_A^{tele} = \hat{X}_A^{out} + g_X(y_s - q_c) = \hat{X}_A^{out} + \frac{1}{\sqrt{2}}g_X(\hat{y}_s^{out} - \hat{q}_c^{out}) + g_X\hat{Y}$$
$$\hat{P}_A^{tele} = \hat{P}_A^{out} - g_P(y_c + q_s) = \hat{P}_A^{out} - \frac{1}{\sqrt{2}}g_P(\hat{y}_c^{out} + \hat{q}_s^{out}) + g_P\hat{Q} \quad (3)$$

where $g_{X,P}$ are the feedback gains. This step completes the teleportation protocol, as the light operators $\hat{Y}, \hat{Q}$ are now transferred onto atomic operators $\hat{X}_A^{tele}, \hat{P}_A^{tele}$, and all other terms in equation (3) can be made small with a suitable choice of κ and g.

To prove that we have performed the quantum teleportation, we determine the fidelity of the teleportation. Towards this end, we send a second—verifying—strong pulse of y-polarized light through the

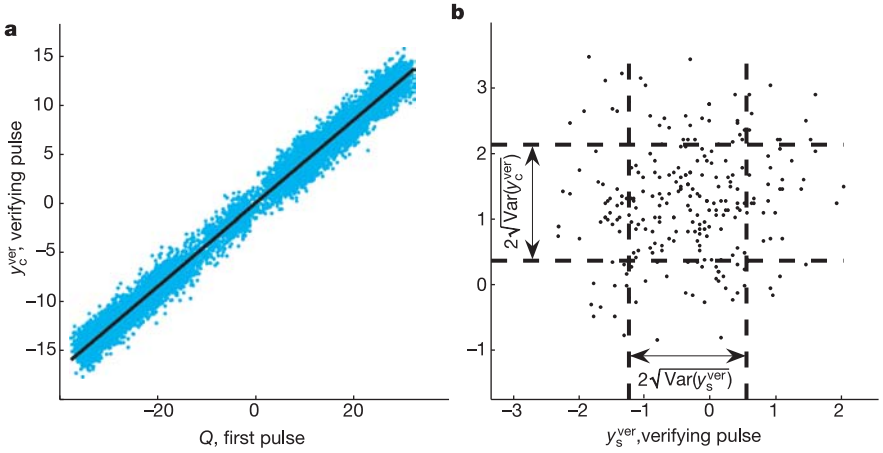

Figure 2 | Raw experimental data for a series of teleportation runs. **a**, Calibration of the teleportation feedback gain. Verifying pulse canonical variable y_c^{ver} versus the input pulse canonical variable Q for 10,000 teleportation runs. All dimensionless canonical variables are normalized so that their variance for a vacuum state is 1/2. The coherent input state used in the plot has a mean photon number of $\bar{n} \approx 500$, and is slowly modulated in phase during this measurement. The straight line fit is used for calibration of the feedback gain (see comments in the text). **b**, An example of data from which the atomic state variances after the teleportation are determined. Two canonical variables of the verifying pulse, y_c^{ver} and y_s^{ver}, are plotted for an input state with $\bar{n} = 5$ and a fixed phase. The dashed lines indicate twice the standard deviation intervals $2\sqrt{\mathrm{Var}(y_{c,s}^{ver})}$ which are used to determine the atomic state variances as discussed in the text.

atomic ensemble after the teleportation is completed. From this measurement we reconstruct the atomic operators $\hat{X}_{\mathrm{A}}^{\mathrm{tele}}$ and $\hat{P}_{\mathrm{A}}^{\mathrm{tele}}$. The fidelity is the overlap of the input state and the teleported state averaged over the input state distribution[12,14,17]. The classical benchmark fidelity which has to be exceeded in order to claim the success of quantum teleportation is known[11] for a gaussian distribution of coherent states with the width corresponding to the mean photon number $\langle n\rangle$ centred at zero. The experimental fidelity for such distribution can be found as[6,18]:

$$F_n = \frac{2}{\sqrt{\left(2\langle n\rangle(1-g_X)^2+1+2\sigma_X^2\right)\left(2\langle n\rangle(1-g_P)^2+1+2\sigma_P^2\right)}}$$

The gains are defined from the mean values of atomic and light operators: $\bar{X}_{\mathrm{A}}^{\mathrm{tele}} = g_X\bar{Y}$, $\bar{P}_{\mathrm{A}}^{\mathrm{tele}} = g_P\bar{Q}$. σ_X^2, σ_P^2 are the variances for the final gaussian state of the atoms.

The mean values for the input light operators are determined from the results of the Bell measurement: $\bar{y}_{\mathrm{s}} - \bar{q}_{\mathrm{c}} = \bar{Y}$ and $\bar{y}_{\mathrm{c}} + \bar{q}_{\mathrm{s}} = \bar{Q}$. The mean values and the variances of the atomic operators are determined from the verifying pulse measurements. Using equations (1) and (3) and the input–output beamsplitter relations[12], we can link the measurement of the verifying pulse on the S_2detector to the atomic mean values: $\bar{y}_{\mathrm{c}}^{\mathrm{ver}} = \frac{\kappa}{2}\bar{P}_{\mathrm{A}}^{\mathrm{tele}} = \frac{g_P\kappa}{2}\bar{Q}$, $\bar{y}_{\mathrm{s}}^{\mathrm{ver}} = \frac{\kappa}{2}\bar{X}_{\mathrm{A}}^{\mathrm{tele}} = \frac{g_X\kappa}{2}\bar{Y}$. Using these expressions, we can calibrate $g_{X,P}$, as shown in Fig. 2a where $\hat{y}_{\mathrm{c}}^{\mathrm{ver}}$ is plotted as a function of $\hat{Q}$, as the value of $\kappa = 0.93$ is determined independently from the projection noise measurement (see Methods). From the linear fit to this distribution we find g_P, which can then be tuned to a desired value electronically. Results plotted in Fig. 2a along with similar results for the other operator $\bar{y}_{\mathrm{s}}(\bar{Y})$ present the proof of the successful classical transfer of the mean values of the quantum mechanical operators $\hat{Y}, \hat{Q}$ of light onto atomic operators.

To verify the success of the quantum teleportation, we have to determine the variances of the two atomic operators which now contain the teleported input light operators. Figure 2b shows an example of results $\hat{y}_{\mathrm{c}}^{\mathrm{ver}}, \hat{y}_{\mathrm{s}}^{\mathrm{ver}}$ for 250 teleportation runs for a fixed input state. Making use of equation (1) and the beamsplitter relations, we can directly find the atomic state variances from $\mathrm{Var}\{\hat{y}_{\mathrm{s(c)}}\}$ of such distribution as $\sigma_{X(P)}^2 = \frac{4}{\kappa^2}\left[\mathrm{Var}\{\hat{y}_{\mathrm{s(c)}}\} - \frac{\kappa^4}{48} - \frac{1}{2}\right]$. The final values of σ_X^2, σ_P^2 for a coherent state with a varied phase and a given $\bar{n}$ are found as averages over 10,000 points (that is, 40 runs like in Fig. 2b). For example, for $\bar{n} = 5$ we find $\sigma_{X(P)}^2 = 1.20(1.12)$ taken at gains 0.96 and 0.95 respectively. The results of $\sigma_{X,P}^2(g_{X,P})$ for a range of photon numbers $\bar{n} = 0$(vacuum), $\bar{n} = 5$, 20, 45, 180, 500 at various gains are summarized in a figure in the Supplementary Methods. From this we obtain $\sigma_{X,P}^2(g_{X,P})$, which can be inserted into the fidelity expression. For a given width of the gaussian distribution of coherent states we find the values of g_X, g_P, and the corresponding $\sigma_{X,P}^2(g_{X,P})$ which maximize the fidelity. We obtain the following fidelities for distributions with a width $\langle n\rangle = 2$, 5, 10, 20, 200: $F_2 = 0.64 \pm 0.02$; $F_5 = 0.60 \pm 0.02$; $F_{10} = 0.59 \pm 0.02$; $F_{20} = 0.58 \pm 0.02$; $F_{200} = 0.56 \pm 0.03$. The expression for the classical benchmark fidelity[11] $F_n^{\mathrm{class}} = \frac{\langle n\rangle+1}{2\langle n\rangle+1}$ gives $F_2^{\mathrm{class}} = 0.60$; $F_5^{\mathrm{class}} = 0.545$; $F_{10}^{\mathrm{class}} = 0.52$; $F_{20}^{\mathrm{class}} = 0.51$; $F_{200}^{\mathrm{class}} = 0.50$ (see Supplementary Methods for details on the fidelity calculations). The maximal $\langle n\rangle$ for successful teleportation is limited by small fluctuations of the classical gain, which for large $\bar{n}$ lead to large uncontrolled displacements of the teleported state with respect to the input state, and hence to the decrease in the fidelity.

In Fig. 3 we show the tomographically reconstructed teleported state with the mean photon number $\bar{n} = 5$. Owing to the gaussian character of the state, the knowledge of the means and the variances of two quadrature phase operators is sufficient for the reconstruction.

Note that the atomic object onto which the teleportation is performed contains hundreds of billions of atoms. However, the number of excitations in the ensemble, of course, corresponds to the number of photons in the initial state of light. Those excitations are coherently distributed over the entire ensemble.

Having demonstrated the teleportation for gaussian states, we now address the applicability of this teleportation protocol to the teleportation of a light qubit, which is relevant for, for example, quantum computing[3]. In the Supplementary Notes we give the derivation of the predicted qubit fidelity, F_{q}, based on the performance of our teleportation protocol for coherent states. For experimentally relevant values of losses and decoherence, $F_{\mathrm{q}} = 0.72$—higher than the best classical fidelity for a qubit of 0.67—can be predicted. In order to experimentally demonstrate such qubit teleportation, a source generating such a qubit in a temporal, spectral and spatial mode compatible with our atomic target is required. First steps towards generation of an atom-compatible qubit state of light have been recently made using atomic ensembles[19–21], single atoms in a cavity[22,23], and a photon subtracted squeezed state[24].

In our experiment, the entanglement generation and the Bell measurement overlap in time because the duration of the strong pulse and the pulse to be teleported is 2 ms, which is much longer than the time it takes light to travel from Alice to Bob. This situation, also the case in some teleportation experiments[6,8], is different, for example, from the teleportation[7,9,10] in which the entanglement generation and the Bell measurement are separated in time. This feature is not inherent to our teleportation scheme—indeed, in principle, a shorter strong pulse (of higher power) would generate the same entanglement on a timescale short compared to the propagation time, especially if the distance from Alice to Bob is extended to a few kilometres. The teleportation distance can be increased, and is limited only by propagation losses of light and the atomic coherence lifetime. The timing of the entanglement generation and the Bell measurement may be potentially important for future applications.

Further improvement of the present teleportation protocol can be achieved by performing more complex photocurrent processing with the same homodyne set-up. As shown in ref. 12 and in the Supplementary Notes, a fidelity of 0.93 can be achieved if such processing is combined with the use of an experimentally feasible[25] 6 dB squeezed strong pulse.

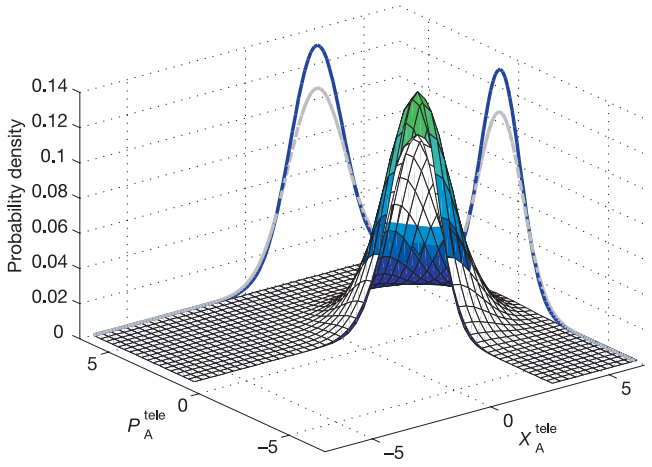

Figure 3 | Tomographic reconstruction of a teleported state with $\bar{n} = 5$ (coloured contour) versus the state corresponding to the best classical state transfer. Canonical variables plotted on horizontal axes are normalized so that their variance for a vacuum state is 1/2.

METHODS

Calibration and measurement techniques. Physically, we perform measurements of the Stokes operators of light by two sets of balanced homodyne detectors (Fig. 1). The measurements on the first pulse represent the generalized Bell measurement. The same measurements on the second (verifying) pulse allow us to determine the teleported atomic state by performing quantum state

tomography. The relevant $\cos(\Omega t)$ and $\sin(\Omega t)$ modulation components of the Stokes operators are measured by processing the corresponding photocurrents with lock-in amplifiers. The Stokes operators of interest are $\hat{S}_2$ (which is the difference between photon fluxes in the modes polarized at $\pm 45°$ to the vertical axis, and $\hat{S}_3$ (which is the corresponding quantity for the left- and right-hand circular polarizations).

Calibration of the measurement of canonical variables for light is based on measurements of the shot (vacuum) noise level. We measure the Stokes parameters for the *x*-polarization mode in a vacuum state. The linear dependence of the variance of the measured photocurrents on the optical power of the strong pulse proves that the polarization state of light is, in fact, shot (vacuum) noise limited[25]. All other measurements of $\hat{S}_2, \hat{S}_3$ are then normalized to this shot noise level, yielding the canonical variables as:

$$y_c = \frac{1}{\sqrt{2}\int_0^T \mathrm{d}\tau \cos(\Omega t) S_2^{\mathrm{vacuum}}(\tau)} \int_0^T \mathrm{d}\tau \cos(\Omega t) S_2(\tau)$$

and similarly for $q_c(S_3)$and the $\sin(\Omega t)$ components. Since our detectors have nearly unity (better than 0.97) quantum efficiency, the Stokes operators can be operationally substituted with measured photocurrents.

Next we need to calibrate the atomic coherent (projection) noise level. Whereas balanced homodyne detection for light has become an established technique for determination of the vacuum state[6], a comparable technique for atoms is a relatively recent invention. Here we utilize the same procedure as used in our previous experiments on the atoms–light quantum interface[14,15]. We use the fact that the vacuum (projection) noise level for collective atomic spin states in the presence of a bias magnetic field can be determined by sending a pulse of light through two identical atomic ensembles with oppositely oriented macroscopic spin orientation. We therefore insert a second atomic cell in the beam. As described in detail in ref. 15, the transmitted light state in this experiment is given by:

$$\hat{y}_{\mathrm{c}}^{\mathrm{out}} = \hat{y}_{\mathrm{c}}^{\mathrm{in}} + \frac{\kappa}{\sqrt{2}}\left(\hat{P}_{\mathrm{atom1}} + \hat{P}_{\mathrm{atom2}}\right) = \hat{y}_{\mathrm{c}}^{\mathrm{in}} + \kappa \hat{P}_{\mathrm{total}}$$

where $\hat{P}_{\mathrm{total}}$ is the spin canonical variable for the entire 2-cell atomic sample. Intuitively this equation can be understood by noting that terms proportional to κ^2 in equation (1) cancel out for propagation through two oppositely oriented ensembles. A similar equation holds for $\hat{y}_{\mathrm{s}}^{\mathrm{out}}$ with substitution of $\hat{X}_{\mathrm{total}}$ for $\hat{P}_{\mathrm{total}}$. The results for $\mathrm{Var}(\hat{y}_{\mathrm{c,s}}^{\mathrm{out}})$ as a function of the number of atoms are shown in the figure in the Supplementary Methods. The fact that the points lie on a straight line, along with the independent measurement of the degree of spin polarization above 0.99, proves[14,15,18] that we are indeed measuring the vacuum (projection) noise of the atomic ensemble. κ^2 for different atomic numbers is then calculated from the graph (Supplementary Methods). Its values are in good agreement with the theoretical calculation[18] according to $\kappa = a_1\sqrt{N_{\mathrm{ph}}N_{\mathrm{at}}F\sigma\Gamma/A\Delta}$. In the experiment, we monitor the number of atoms by sending a weak off-resonant probe pulse along the direction *x* and measuring the Faraday rotation angle proportional to the collective macroscopic spin of the ensemble $J_x = 4N_{\mathrm{at}}$. This Faraday angle is monitored throughout the teleportation experiment, so that the value of κ^2 is known at every stage.

Decoherence and losses. The main sources of imperfections are decoherence of the atomic state and reflection losses of light. For experimental values of the atomic decoherence and losses, the model developed in ref. 12 predicts, for example, $F_5 = 0.66$, which is still higher than the observed value owing to imperfections unaccounted for in the model but comparable to the obtained experimental results. Dissipation also affects the experimental state reconstruction procedure. The main effect of the light losses $\varepsilon = 0.09$ is that it modifies κ into $\kappa\sqrt{1-\varepsilon}$. However, this modified κ is, in fact, exactly the parameter measured in the two-cell calibration experiment described above, so no extra correction is due because of these losses. There is also a small amount of electronic noise of detectors which can be treated as an extra vacuum contribution to the input state.

Standard deviation of the teleportation fidelity. The standard deviation of the fidelity for $\langle n\rangle \leq 20$ is calculated as follows:

$$\mathrm{SD}(F) = \sqrt{\delta_{\mathrm{PN}}^2 + \delta_{\mathrm{SN}}^2 + \delta_{\mathrm{el}}^2 + \delta_{\beta}^2 + \delta_{\mathrm{SNR}}^2 + \delta_{\mathrm{fit}}^2 + \delta_g^2} =$$

$$= 10^{-2}\sqrt{1.0^2 + 1.65^2 + 0.1^2 + 0.3^2 + 0.2^2 + 1.2^2 + 0.8^2} \approx 0.02$$

where $\delta_{\mathrm{PN}} = 0.01$ is the contribution to the SD(F) due to the projection noise fluctuations including an error due to imperfect optical pumping, $\delta_{\mathrm{SN}} = 0.017$ is the contribution due to the shot noise level uncertainty, $\delta_{\mathrm{el}} = 0.001$ is the contribution of the electronics noise level fluctuations, $\delta_{\beta} = 0.003$ is the uncertainty due to fluctuations in the atomic decay constant, $\delta_{\mathrm{SNR}} = 0.002$ is the contribution of the fluctuations in the ratio of responses of two pairs of detectors, $\delta_{\mathrm{fit}} = 0.012$ is the deviation due to the uncertainty of the quadratic fit of the atomic noise as a function of gain, and $\delta_g = 0.008$ is the contribution of the gain fluctuations. For $\langle n\rangle > 20$, $\delta_{\mathrm{fit}} = 0.016$, giving SD($F$) $\approx 0.026 \approx 0.03$.

Received 6 May; accepted 28 July 2006.

1. Bennett, C. H. *et al.* Teleporting an unknown quantum state via dual classical and Einstein-Podolsky-Rosen channels. *Phys. Rev. Lett.* **70,** 1895–1899 (1993).
2. Briegel, H. J., Dur, W., Cirac, J. I. & Zoller, P. Quantum repeaters: the role of imperfect local operations in quantum communication. *Phys. Rev. Lett.* **81,** 5932–5935 (1998).
3. Gottesman, D. & Chuang, I. Demonstrating the viability of universal quantum computation using teleportation and single-qubit operations. *Nature* **402,** 390–393 (1999).
4. Bouwmeester, D. *et al.* Experimental quantum teleportation. *Nature* **390,** 575–579 (1997).
5. Boschi, D., Branca, S., De Martini, F., Hardy, L. & Popescu, S. Experimental realization of teleporting an unknown pure quantum state via dual classical and Einstein-Podolsky-Rosen channels. *Phys. Rev. Lett.* **80,** 1121–1125 (1998).
6. Furusawa, A. *et al.* Unconditional quantum teleportation. *Sci. Tech. Froid* **282,** 706–709 (1998).
7. de Riedmatten, H. *et al.* Long distance quantum teleportation in a quantum relay configuration. *Phys. Rev. Lett.* **92,** 047904 (2004).
8. Takei, N., Yonezawa, H., Aoki, T. & Furusawa, A. High-fidelity teleportation beyond the no-cloning limit and entanglement swapping for continuous variables. *Phys. Rev. Lett.* **94,** 220502 (2005).
9. Barrett, M. D. *et al.* Deterministic quantum teleportation of atomic qubits. *Nature* **429,** 737–739 (2004).
10. Riebe, M. *et al.* Deterministic quantum teleportation with atoms. *Nature* **429,** 734–737 (2004).
11. Hammerer, K., Wolf, M. M., Polzik, E. S. & Cirac, J. I. Quantum benchmark for storage and transmission of coherent states. *Phys. Rev. Lett.* **94,** 150503 (2005).
12. Hammerer, K., Polzik, E. S. & Cirac, J. I. Teleportation and spin squeezing utilizing multimode entanglement of light with atoms. *Phys. Rev. A* **72,** 052313 (2005).
13. Vaidman, L. Teleportation of quantum states. *Phys. Rev. A* **49,** 1473–1476 (1994).
14. Julsgaard, B., Sherson, J., Fiurášek, J., Cirac, J. I. & Polzik, E. S. Experimental demonstration of quantum memory for light. *Nature* **432,** 482–486 (2004).
15. Julsgaard, B., Kozhekin, A. & Polzik, E. S. Experimental long-lived entanglement of two macroscopic objects. *Nature* **413,** 400–403 (2001).
16. Julsgaard, B., Schori, C., Sørensen, J. L. & Polzik, E. S. Atomic spins as a storage medium for quantum fluctuations of light. *Quant. Inf. Comput.* **3** (special issue), 518–534 (2003).
17. Julsgaaard, B., Sherson, J., Sørensen, J. L. & Polzik, E. S. Characterizing the spin state of an atomic ensemble using the magneto-optical resonance method. *J. Opt. B* **6,** 5–14 (2004).
18. Sherson, J., Julsgaaard, B. & Polzik, E. S. Deterministic atom-light quantum interface. *Adv. At. Mol. Opt. Phys.* (in the press); preprint at ⟨http://arxiv.org/quant-ph/0601186⟩ (2006).
19. Chou, C. W., Polyakov, S. V., Kuzmich, A. & Kimble, H. J. Single-photon generation from stored excitation in an atomic ensemble. *Phys. Rev. Lett.* **92,** 213601 (2004).
20. Chaneliere, T. *et al.* Storage and retrieval of single photons transmitted between remote quantum memories. *Nature* **438,** 833–836 (2005).
21. Eisaman, M. D. *et al.* Electromagnetically induced transparency with tunable single-photon pulses. *Nature* **438,** 837–841 (2005).
22. Kuhn, A., Hennrich, M. & Rempe, G. Deterministic single-photon source for distributed quantum networking. *Phys. Rev. Lett.* **89,** 067901 (2002).
23. McKeever, J. *et al.* Deterministic generation of single photons from one atom trapped in a cavity. *Science* **303,** 1992–1994 (2004).
24. Neergaard-Nielsen, J. S., Melholt Nielsen, B., Hettich, C., Mølmer, K. & Polzik, E. S. Generation of a superposition of odd photon number states for quantum information networks. *Phys. Rev. Lett.* **97,** 083604 (2006).
25. Polzik, E. S., Carri, J. & Kimble, H. J. Spectroscopy with squeezed light. *Phys. Rev. Lett.* **68,** 3020–3023 (1992).

Supplementary Information is linked to the online version of the paper at www.nature.com/nature.

Acknowledgements The experiment was performed at the Niels Bohr Institute, and was funded by the Danish National Research Foundation through the Center for Quantum Optics (QUANTOP), by EU grants COVAQIAL and QAP, and by the Carlsberg Foundation. I.C. and E.S.P. acknowledge the hospitality of the Institut de Ciències Fotòniques (ICFO) in Barcelona where ideas leading to this work were first discussed. The permanent address of K.H. is the Institut für theoretische Physik, Innsbruck, Austria.

Author Information Reprints and permissions information is available at www.nature.com/reprints. The authors declare no competing financial interests. Correspondence and requests for materials should be addressed to E.S.P. (polzik@nbi.dk).